Available on CMS information server **CMS AN-NOTE 2010/292**

CMS Analysis Note

The content of this note is intended for CMS internal use and distribution only

March 22, 2011

Photon Efficiency Measurements using Tag and Probe

M. Sani[a)], S. Simon[a)], M. Pieri[a)], J. Branson[a)], E. Sudano[a)], C. Palmer[a)], A. Holzner[a)]

a) University of California, San Diego

Abstract

A measurement of photon identification efficiency is presented in this note. The sample of electrons from Z decays belonging to the first 35 pb^{-1} of data collected by the CMS experiment has been used to evaluate the performance of different photon selections on the corresponding calorimetric clusters using the Tag and Probe technique.

Contents

1 Introduction

Simulation of the detector response has traditionally been the tool to determine reconstruction efficiencies for physics objects such as leptons, photons, jets, missing energy etc. Such simulations always have limited precision, and, especially in the start-up phase of an experiment, very little or no tuning of the simulation to the observed data has been performed. It is thus very important to determine selection efficiency from recorded collisions.

Direct measurement of photon selection efficiencies is limited by the low statistics of $Z \rightarrow \mu\mu\gamma$ events in early data. However, since electrons and photons have similar shower development in the calorimeter, the Tag and Probe method on Z→ee events [1] can be used to determine the relative efficiencies in data and MC, which can then be used to correct photon efficiencies measured in MC. Using this technique the probe electrons are treated as photons and the electron Super-Cluster is requiresd to pass photon selection cuts.

The Note is organized in the following manner: in Section 2 a brief description of the used samples is given; a detailed description of the method and the event selections are outlined in Section 3; the results are discussed and presented as a function of various photon and electron variables ($\mathrm{E_T}$, η, R9 and fBrem) in Section 4. In the Appendices further results are reported.

2 Samples

The present study has been carried the first time using `CMSSW_3_6_X`. The same analysis has been repeated and updated using `CMSSW_3_8_X` and `CMSSW_3_9_X`. In the following subsections, data and MC samples used for the latest version of study are presented. The details of the older analysis are reported in the Appendix A.

2.1 Data

The data used for this analysis consist of the full dataset (35 pb^{-1}) recorded by the CMS detector at $\sqrt{s}$ = 7 TeV in 2010. The specific datasets used are defined in Table 1.

The official JSON files (Cert_136033-149442_7TeV_XXXReReco_Collision10_JSON.txt) were used to select good lumi sections from these runs (XXX corresponds to the different label of rereco samples e.g Dec22, Nov4).

2.2 Monte Carlo

Monte Carlo samples from the Fall10 `CMSSW_3_8_X` and Winter10 `CMSSW_3_9_X` re-digitization were used. The signal and background were all generated with `PYTHIA` [2]. Table 2 shows the samples and equivalent integrated luminosities used. All cross sections used are LO PYTHIA cross sections except the Drell-Yan→ee signal sample for which the NLO k-factor, 1.2275, was applied.

Table 1: Run ranges and corresponding datasets used in the analysis (XXX corresponds to the different label of rereco samples e.g Dec22, Nov4).

Run Range	Dataset Name
132440 - 144114	/EG/Run2010A-XXXReReco_v2/RECO
146428 - 149294	/Electron/Run2010B-XXXReReco-v2/RECO

Table 2: List of Monte Carlo samples used in the analysis. The corresponding integrated luminosity is also reported.

Process	$\hat{p_t}$ range (GeV/c)	$\int Ldt$ (pb^{-1})
Drell-Yan→ee (Signal)		125.3
W →eν		26.5
Photon + Jet	$15-30$	6.2
Photon + Jet	$30-50$	42.2
Photon + Jet	$30-80$	6.2
Photon + Jet	$80-120$	42.2
QCD bc→e	$20-30$	8.7
QCD bc→e	$30-80$	6.7
QCD bc→e	$80-170$	106.1
QCD EM Enriched	$20-30$	13.1
QCD EM Enriched	$30-80$	11.3
QCD EM Enriched	$80-170$	38.3

3 Selections

In the process of measuring the efficiency of a given photon selection we have also checked the consistency among different data-driven techniques. In particular we concentrated on three different methods: simple counting method, invariant mass distribution fits and opposite-sign same-sign. In the following paragraphs each method is described separately while the corresponding results are presented in the next Section 4. The requirements for the tag and probe electrons, as well as the variables and thresholds for the studied photon selections are described at the end of the present Section.

3.1 General Description of the Method

The Tag and Probe technique requires that one electron of the Z decay is well identified ("tag"). The second leg of the decay has to pass less stringent requirements ("probe"). Then the tag and probe electrons are required to have a reconstructed invariant mass compatible with the Z mass.

The selection efficiency is estimated as the ratio of the number of probes passing the cuts to the total number of probes. In order to determine efficiency for photons on an electron sample, we take the reconstructed photon candidate in the event which is made of the same Super-Cluster as the probe electron. Tag and probe on Z→ee events yields a very clean sample.

By Pixel-Match efficiency we mean the probability for a reconstructed photon to have compatible hits in the Pixel sub-detector. This is an important requirement to discriminate electrons from photons and to give an estimate of the photon fake-rate from electrons. The Tag and Probe technique has been also used to estimate Pixel-Match efficiency in data.

3.1.1 Counting Method

This is the simplest method that we have studied. The low background contamination allows for the counting method to be employed. The number of passing and failing signal events is determined by simply counting the data entries in invariant mass window around the nominal Z mass (i.e. 50-120 GeV/c^2).

The remaining background after the tag and probe selection, which is low but not negligible, is estimated from MC and the corresponding number of events is subtracted from the data.

In order to further reduce the effect of the background we assume that the overall photon selection efficiency can be written as a product of efficiencies of complementary subsets of the selection cuts which are measured separately. This has the advantage that we can significantly increase the sample purity reducing at the same time the statistical uncertainties on the efficiency.

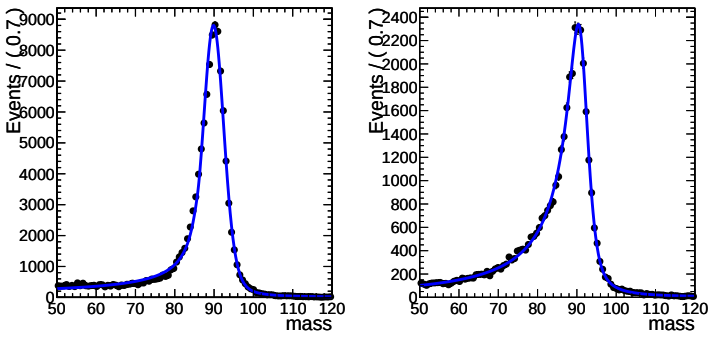

(a)

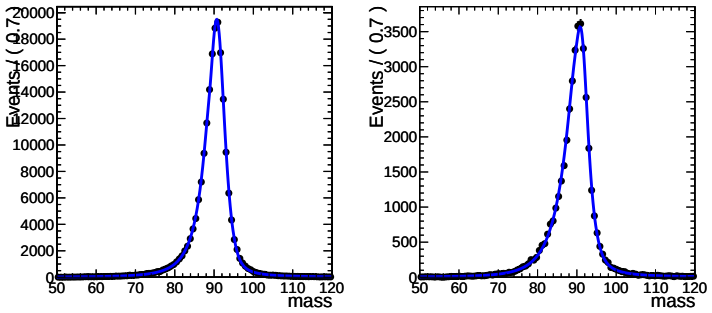

(b)

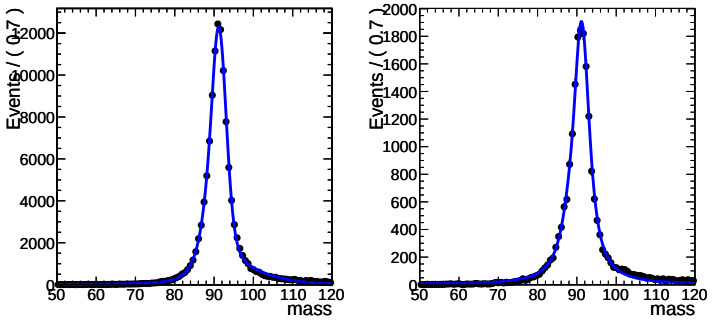

(c)

Figure 1: Fit to Z MC passing (left) and failing (right) distributions: (a) $20 < E_T < 35$ (b) $35 < E_T < 45$ (c) $E_T > 45$. The line represents Breit Wigner convoluted with the modified Crystal-Ball function resulting from the fit.

3.1.2 Fits

An alternative way to determine the number of passing and failing signal events is to perform fits to the electron invariant mass distribution in the pass and fail samples determining at the same time the signal and background yields.

The first step is to determine signal passing and failing shapes by fitting the MC Z distribution with the convolution of a Breit Wigner and a Crystal-Ball modified to include an extra half Gaussian on the high end tail.

Then the data distributions are fitted with the sum of this MC determined shape (where the Crystal-Ball tail is fixed) and an exponential to take into account the background contribution. In this case it is possible to reasonably estimate the contribution to the left tail of the distribution given by signal events.

Figures 1 and 2 show examples of fits to MC distribution.

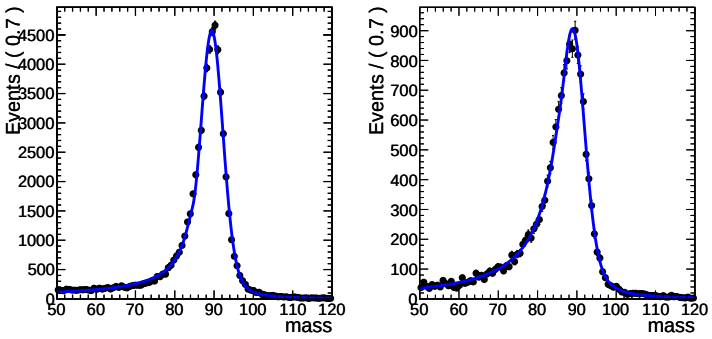

(a)

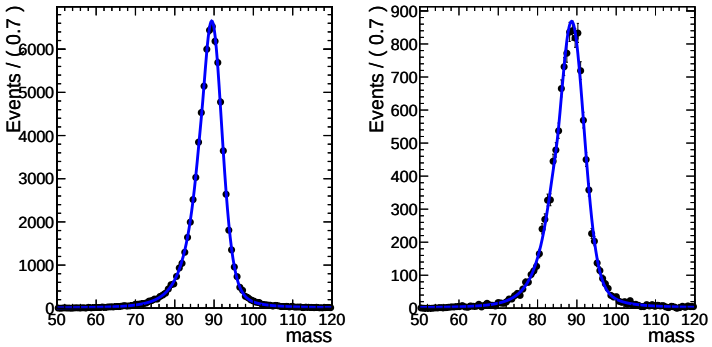

(b)

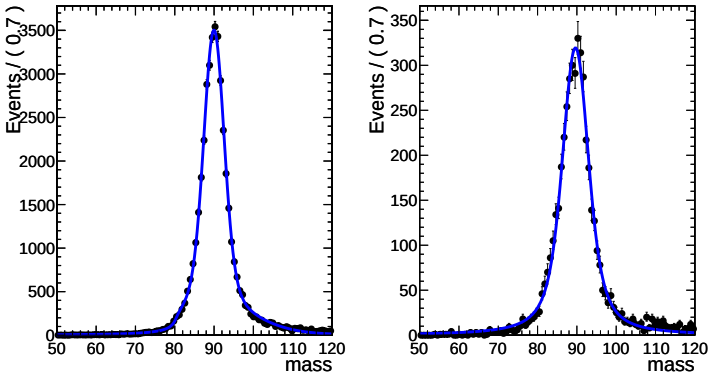

(c)

Figure 2: Fit to Z MC passing (left) and failing (right) distributions: (a) $20 < E_T < 35$ (b) $35 < E_T < 45$ (c) $E_T > 45$. The line represents Breit Wigner convoluted with the modified Crystal-Ball function resulting from the fit.

3.1.3 Opposite-Sign Same-Sign

The third method that we have studied consists on treating separately opposite-sign and same-sign electron pairs. Other details of this method can be found in [6].

The background subtracted number of signal events can then be determined as:

$$N_S = \frac{(N_{OS} - N_{SS})}{(1 - 2q_{misid})^2} - (N_{OS}^B - N_{SS}^B) \tag{1}$$

where N_{OS} and N_{SS} are the opposite and same-sign number of data events, q_{misid} is the charge mis-identification probability and N_{OS}^B and N_{SS}^B are the number of background opposite and same-sign events. N_S is then computed for passing and failing events to compute the final efficiency.

Since the charge mis-identification probability cannot be easily determined from data for the same-sign category we decided to get it directly from MC as well as N_{OS}^B and N_{SS}^B. Also we used two different estimates for the charge mis-identification probability for passing and failing events using the following formula:

$$q_{misid} = \frac{1 - \sqrt{|q_1 q_2|}}{2} \tag{2}$$

3.2 Tag and Probe Definitions

Both barrel and endcap electrons, excluding transition region (i.e. having $|\eta| < 1.4442$ and $|\eta| > 1.566$, where η is determined by the photon Super-Cluster position), are considered.

The tag electron is required to have $\mathrm{E_T} > 20$ GeV and to pass the "SuperTight" selection of the Cuts in Categories electron ID [7]. The probe is defined as a reconstructed electron having $\mathrm{E_T} > 20$ GeV.

To compute factorized efficiencies, in the counting method, we have split the cuts into two sets (isolation cuts and H/E - $\sigma_{i\eta i\eta}$) and measured the efficiency of the two selection separately. The probes were also required to pass in turn one of the two set of cuts. Then the two measurements have been combined to get the total selection efficiency. Possible correlations between the two sets of cuts are taken into account by correcting the final result as described in the Section 4.

3.2.1 Pixel Match Efficiency

The Tag and Probe technique has been also used to estimate Pixel-Match efficiency in data. In this case the requirements on the tag electron are the same described above. Instead we have used and alternate definition for the probe with no electron ID requirements: a probe is just a reconstructed photon (a SuperCluster) passing photon identification cuts with $\mathrm{E_T} > 20$ GeV.

3.3 Photon Identification

The photon identification is based on the following variables:

- H/E: fraction of hadronic over electromagnetic energy inside a cone of ΔR = 0.15 around photon direction.
- $\sigma_{i\eta i\eta}$: transverse shape of the electromagnetic cluster computed with logarithmic weights as

$$\sigma_{i\eta i\eta}^2 = \frac{\sum_i^{5\times5} w_i(\eta_i - \bar{\eta}_{5\times5})^2}{\sum_i^{5\times5} w_i}, \qquad w_i = max(0, 4.7 + ln\frac{E_i}{E_{5\times5}}) \tag{3}$$

  where E_i and η_i are the energy and pseudorapidity of the ith crystal within 5×5 electromagnetic cluster and $\mathrm{E}_{5\times5}$ and $\eta_{5\times5}$ are the energy and the pseudorapidity of the entire 5×5 cluster.

- Tracker Isolation: computed as the sum of the transverse momenta of all the tracks in a full cone ($\Delta\mathrm{R}_O = 0.4$) centered around a line joining the primary vertex to the cluster. Tracks in an inner cone ($\Delta\mathrm{R}_I = 0.04$) and η-slice ($\Delta\eta$ = 0.015) are not included to avoid misidentification of converted photons. In addition, tracks with a transverse (longitudinal) impact parameter above 0.1 (0.2) cm are also not included.

- ECAL Isolation: computed as the E_T sum of the energy deposits in the approximately 1250 individual crystals located in a cone ($\Delta R_O = 0.4$), centered around the Super-Cluster with a veto cone ($\Delta R_I = 3.5$ crystals) and η-slice ($\Delta\eta$ = 2.5 crystals).

- HCAL Isolation: computed as the sum of the transverse energy in the HCAL towers in a hollow cone with inner radius of $\Delta R_I = 0.15$ and an outer radius of $\Delta R_O = 0.4$ that is centered around the photon Super-Cluster.

The distribution of some of the variables used in the selection for probe electrons are shown in Figures 3 and 4. The differences between data and MC are mainly due to the Pileup. MC events are normalized to the integrated luminosity used in the analysis.

In this study we have considered various sets of selection criteria which are described in the following sections.

3.4 Selection Definition

- CMSSW_3_6_X Photon ID: it is described in detail in [3]. It is made of two set of cuts: a loose one with a relatively high efficiency (about 90%) with minimal impact on the systematics and a tight set which allows powerful background rejection keeping a reasonably high efficiency (about 70%).

- Exotica Photon ID: it corresponds to the tight set of cuts recommended by the EGamma POG.

- Hgg Photon ID: it is currently used in the H$\rightarrow\gamma\gamma$ cut-based analysis.

- Conversion: it is described in detail in [4].

- Combined Isolation: it is described in detail in [5].

The exact definition of the cuts is reported in Table 3.

Table 3: Cuts of the different selection studied in this Note.

Variable	EG Loose	EG Tight	Exotica	Hgg	Conversion	Combined Iso
Ecal+Hcal+Tk	-	-	-	-	-	5
H/E	0.05	0.03	0.05	0.03	0.05	0.05
Tracker Isolation	2.0	0.9	2.0+0.001*p_T	1.5+0.001*p_T	2.0+0.001*p_T	-
ECAL Isolation	4.2	2.4	4.2+0.006*p_T	2.0+0.006*p_T	4.2+0.003*p_T	-
HCAL Isolation	2.2	1.0	2.2+0.0025*p_T	2.0+0.0025*p_T	2.2+0.001*p_T	-
$\sigma_{i\eta i\eta}$	0.01 (0.03)	0.01 (0.028)	0.013 (0.03)	0.01 (0.028)	0.01 (0.03)	0.01 (0.03)

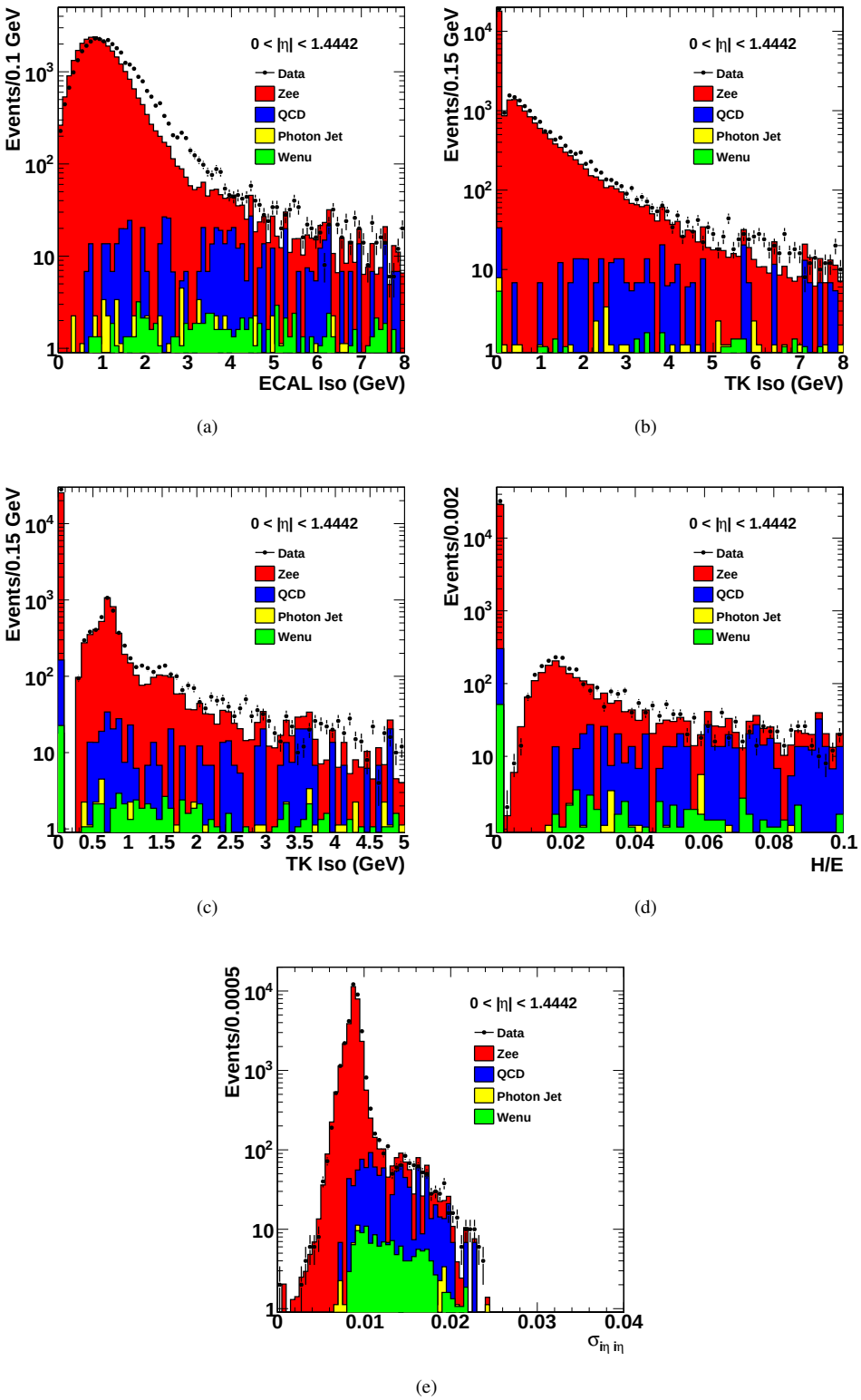

Figure 3: Barrel distributions of the variables used in the photon selection for probe electrons: (a) ECAL Isolation, (b) Tracker Isolation, (c) HCAL Isolation, (d) H/E and (e) $\sigma_{i\eta i\eta}$. The contribution of the different channels is also shown. MC events are normalized to the total integrated luminosity used in the analysis.

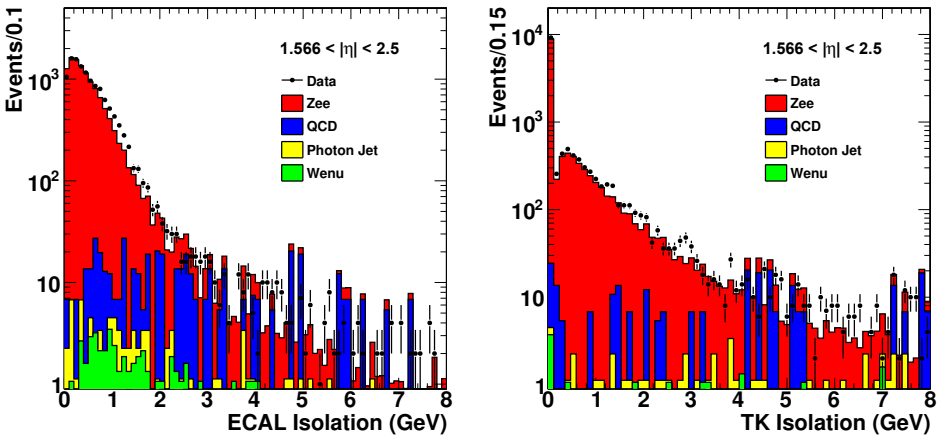

(a)

(b)

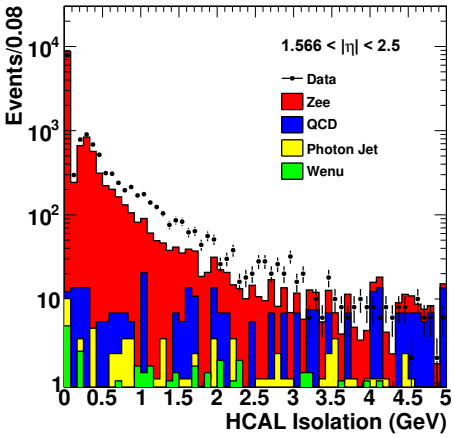

(c)

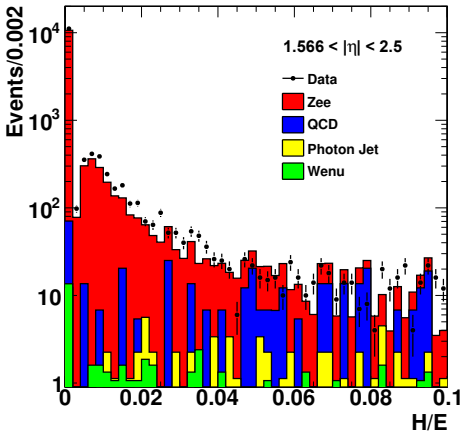

(d)

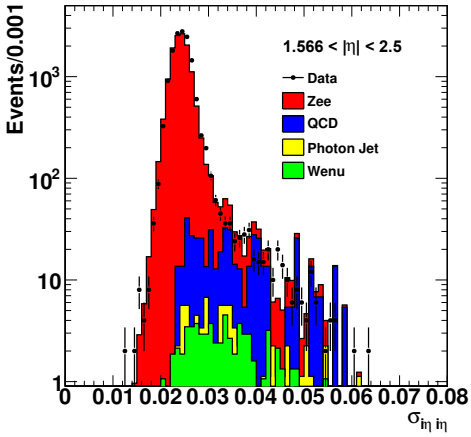

(e)

Figure 4: Endcap distributions of the variables used in the photon selection for probe electrons: (a) ECAL Isolation, (b) Tracker Isolation, (c) HCAL Isolation, (d) H/E and (e) $\sigma_{i\eta i\eta}$. The contribution of the different channels is also shown. MC events are normalized to the total integrated luminosity used in the analysis.

4 Results

In this section only the results for the Hgg Photon ID are reported. Tables and Figures concerning other selections are shown in Appendix.

4.1 Counting Method

Tables 4 to 7 show the Hgg Photon ID selection efficiency in different ranges of the photon $\mathrm{E_T}$, η, R9 (the ratio of the energy contained in the 3x3 region around the seed crystal and the total Super-Cluster energy), fBrem (electron bremstrahlung loss estimated with the tracker) in barrel and endcap measured with the counting method.

All the results have been corrected to take into account possible correlations between the two sets of cuts. Correlations are estimated as the difference between the direct and factorized selection efficiency computed on MC (about 1.5%). The uncertainty quoted for the data results is the combination of the binomial statistical error and the systematic error (assumed to be 100% of the background as estimated from MC) and 50% of the estimated correlation given by the factorization.

To correctly apply background subtraction the electron energy has been scaled so that the Z peak in data was centered at the same value of the MC. To determine the appropriate scale factor the Z mass peak in MC and data (after a tight selection on the electrons to remove almost completely the background) have been fitted separately for barrel and endcap.

The observed discrepancy between MC and data efficiencies can be mainly related to the absence of simulated pileup in MC events. Pileup results are presented in Section 4.4.

The selection efficiency has been also checked on MC photons using γ plus jet events. It turns out that the MC Ratio γ/e is about 1.04 in barrel and endcap.

Figure 5 shows the electron invariant mass distributions for events passing (left) and failing (right) the isolation cuts of the Hgg Photon ID selection. The contribution of the different channels estimated from MC is also shown.

4.2 Fit Method

Passing and failing data events have been fitted using the convolution of a Breit Wigner and a Crystal-Ball (with the tail fixed by the MC signal shape) plus an exponential function to take into account the background contribution. The performed extended likelihood fit gives us the signal and background yields which are used to compute the selection efficiency. Figures 6 to 13 show the fit results.

In Tables 8 to 11 are reported the estimated efficiencies as a function of the probe $\mathrm{E_T}$, η, R9 and fBrem. The statistical error is taken from the fit. Concerning the systematic errors we have analyzed three sources separately:

- background shape, its contribution has been estimated changing the fitting function for the background (exponential, polynomial, $1/x^{\alpha}$) and checking the variation of the final efficiency ($\sim 0.5\%$),
- electron energy scale, its contribution has been estimated varying the electron energy within the current expected energy scale uncertainty and computing the new efficiency ($\sim 0.2\%$),
- signal shape, we have performed the fits varying Crystal-Ball tail parameters (the parameters n and α) by 50% with respect to the one given by the MC fit and determined the effect on the final result ($\sim 1\%$).

In this case no factorization is involved and in future we will check if it can help in reducing the final uncertainty on the measurement.

Table 4: Hgg photon selection efficiency computed with counting method as a function of the photon transverse energy in barrel and endcap.

ET	**MC**	**DATA**	R (DATA/MC)
Barrel			
20 - 35	74.98 $\pm$ 0.11%	69.83 $\pm$ 0.61$\pm$ 2.24%	1.071 $\pm$ 0.036
35 - 45	82.43 $\pm$ 0.08%	76.33 $\pm$ 0.48$\pm$ 0.22%	1.081 $\pm$ 0.007
45 - inf	85.75 $\pm$ 0.09%	78.73 $\pm$ 0.62$\pm$ 0.18%	1.090 $\pm$ 0.009
Endcap			
20 - 35	79.46 $\pm$ 0.14%	77.64 $\pm$ 0.74$\pm$ 2.65%	1.022 $\pm$ 0.036
35 - 45	86.56 $\pm$ 0.11%	84.44 $\pm$ 0.67$\pm$ 0.66%	1.024 $\pm$ 0.011
45 - inf	90.04 $\pm$ 0.14%	87.40 $\pm$ 0.90$\pm$ 0.26%	1.030 $\pm$ 0.011

Table 5: Hgg photon selection efficiency computed with counting method as a function of the photon pseudorapidity in barrel and endcap.

η	**MC**	**DATA**	R (DATA/MC)
0 - 0.5	77.55 $\pm$ 0.09 %	69.66 $\pm$ 0.56 $\pm$ 0.75 %	0.898 $\pm$ 0.012
0.5 - 1.0	81.87 $\pm$ 0.09 %	76.56 $\pm$ 0.54 $\pm$ 0.90 %	0.935 $\pm$ 0.013
1.0 - 1.4442	84.69 $\pm$ 0.09 %	80.28 $\pm$ 0.56 $\pm$ 0.84 %	0.948 $\pm$ 0.012
1.566 - 1.8	83.34 $\pm$ 0.14 %	78.85 $\pm$ 0.87 $\pm$ 0.96 %	0.946 $\pm$ 0.015
1.8 - 2.1	82.38 $\pm$ 0.14 %	80.24 $\pm$ 0.79 $\pm$ 1.00 %	0.974 $\pm$ 0.015
2.1 - 2.5	87.74 $\pm$ 0.11 %	86.63 $\pm$ 0.65 $\pm$ 1.89 %	0.987 $\pm$ 0.022

Table 6: Hgg photon selection efficiency computed with counting method as a function of the photon R9 in barrel and endcap.

R9	**MC**	**DATA**	R (DATA/MC)
Barrel			
0 - 0.8	80.36 $\pm$ 0.09 %	75.61 $\pm$ 0.53 $\pm$ 1.80 %	0.941 $\pm$ 0.023
0.80 - 0.94	81.46 $\pm$ 0.09 %	75.03 $\pm$ 0.54 $\pm$ 0.51 %	0.921 $\pm$ 0.009
0.94 - 1.0	81.34 $\pm$ 0.09 %	74.23 $\pm$ 0.61 $\pm$ 0.23 %	0.912 $\pm$ 0.008
Endcap			
0 - 0.8	77.76 $\pm$ 0.20 %	75.89 $\pm$ 1.02 $\pm$ 3.68 %	0.976 $\pm$ 0.049
0.80 - 0.94	83.96 $\pm$ 0.11 %	81.40 $\pm$ 0.67 $\pm$ 1.19 %	0.970 $\pm$ 0.016
0.94 - 1.0	89.01 $\pm$ 0.11 %	87.17 $\pm$ 0.71 $\pm$ 0.19 %	0.979 $\pm$ 0.009

Table 7: Hgg photon selection efficiency computed with counting method as a function of the electron fBrem in barrel and endcap.

fBrem	**MC**	**DATA**	R (DATA/MC)
Barrel			
-0.2 - 0.2	78.35 $\pm$ 0.09 %	71.84 $\pm$ 0.54 $\pm$ 1.54 %	0.917 $\pm$ 0.021
0.2 - 0.6	82.14 $\pm$ 0.09 %	75.84 $\pm$ 0.59 $\pm$ 0.54 %	0.923 $\pm$ 0.009
0.6 - 1.0	83.00 $\pm$ 0.09 %	77.68 $\pm$ 0.54 $\pm$ 0.35 %	0.935 $\pm$ 0.008
Endcap			
-0.2 - 0.2	84.87 $\pm$ 0.19 %	81.86 $\pm$ 1.12 $\pm$ 3.88 %	0.964 $\pm$ 0.046
0.2 - 0.6	85.04 $\pm$ 0.12 %	82.99 $\pm$ 0.71 $\pm$ 1.23 %	0.976 $\pm$ 0.017
0.6 - 1.0	84.11 $\pm$ 0.12 %	81.48 $\pm$ 0.67 $\pm$ 0.62 %	0.969 $\pm$ 0.011

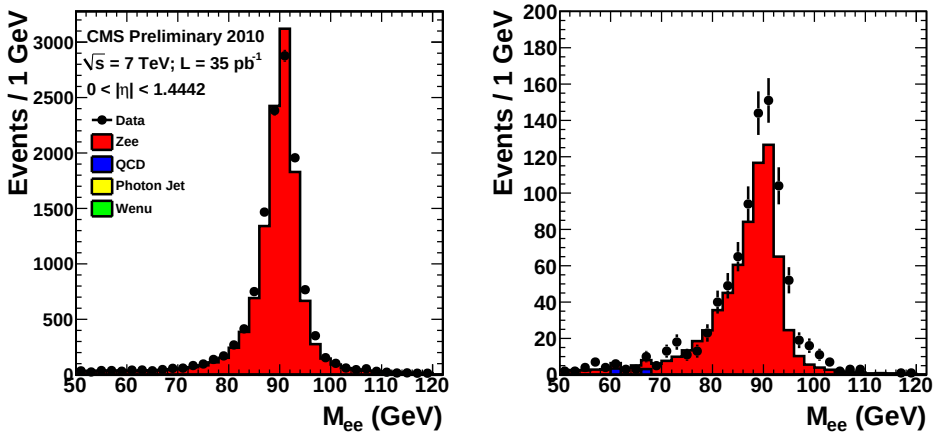

(a)

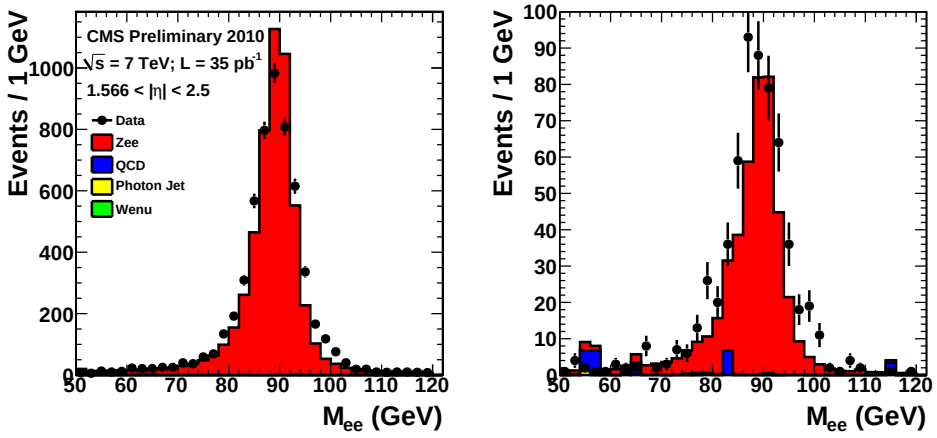

(b)

Figure 5: Electron invariant mass distribution for events passing (left) and failing (right) isolation cuts of the Hgg Photon ID selection in barrel (top) and endcap (bottom). The contribution of the different channels estimated from MC is also shown. MC events are normalized to the total integrated luminosity used in this analysis.

Table 8: Hgg photon selection efficiency computed with fits method as a function of the photon transverse energy in barrel and endcap.

ET	**MC**	**DATA**	R (DATA/MC)
Barrel			
20 - 35	74.98 $\pm$ 0.11%	67.22 $\pm$ 1.20$\pm$ 3.16%	0.897 $\pm$ 0.023
35 - 45	82.43 $\pm$ 0.08%	75.64 $\pm$ 0.59$\pm$ 0.72%	0.917 $\pm$ 0.028
45 - inf	85.75 $\pm$ 0.09%	77.90 $\pm$ 0.76$\pm$ 0.94%	0.908 $\pm$ 0.026
Endcap			
20 - 35	79.46 $\pm$ 0.14%	76.97 $\pm$ 1.29$\pm$ 2.42%	0.969 $\pm$ 0.028
35 - 45	86.56 $\pm$ 0.11%	83.45 $\pm$ 0.81$\pm$ 0.80%	0.964 $\pm$ 0.034
45 - inf	90.04 $\pm$ 0.14%	86.74 $\pm$ 1.06$\pm$ 0.80%	0.963 $\pm$ 0.020

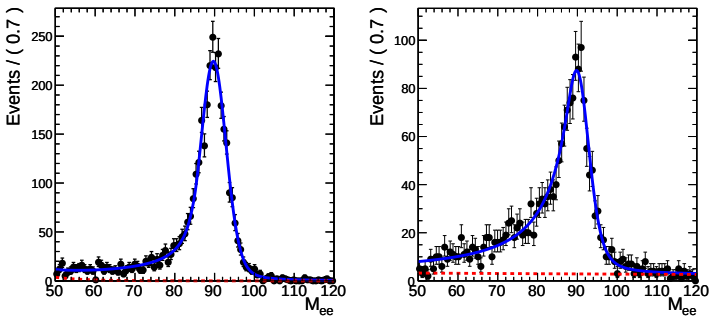

(a)

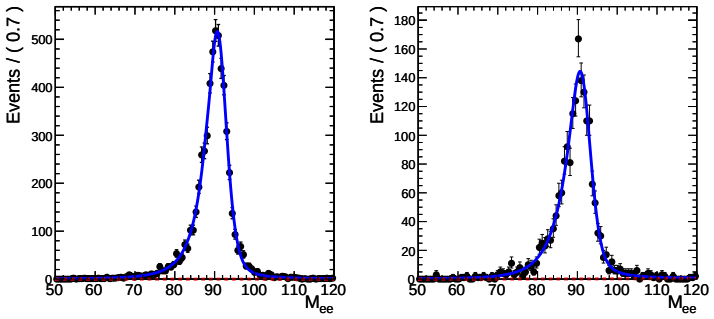

(b)

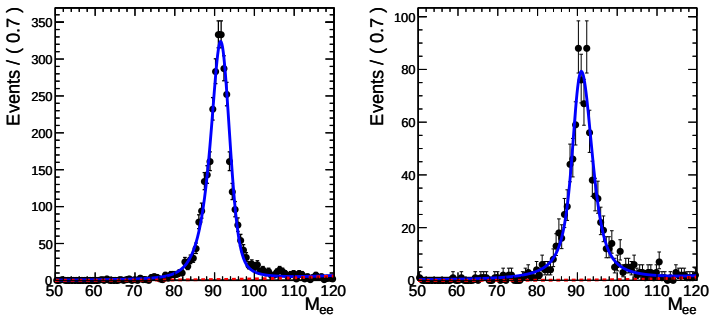

(c)

Figure 6: Fit to passing (left) and failing (right) data, (a) $20 < \mathrm{E_T} < 35$ (b) $35 < \mathrm{E_T} < 45$ (c) $\mathrm{E_T} > 45$.

Table 9: Hgg photon selection efficiency computed with fits method as a function of the photon pseudorapidity in barrel and endcap.

η	**MC**	**DATA**	R (DATA/MC)
0 - 0.5	77.55 ± 0.09 %	$68.73 \pm 0.83 \pm 1.59$ %	0.887 ± 0.023
0.5 - 1.0	81.87 ± 0.09 %	$75.28 \pm 0.79 \pm 2.14$ %	0.919 ± 0.028
1.0 - 1.4442	84.69 ± 0.09 %	$79.45 \pm 0.78 \pm 2.22$ %	0.938 ± 0.028
1.566 - 1.8	83.34 ± 0.14 %	$78.52 \pm 1.20 \pm 1.83$ %	0.943 ± 0.027
1.8 - 2.1	82.38 ± 0.14 %	$80.18 \pm 0.49 \pm 2.82$ %	0.974 ± 0.035
2.1 - 2.5	87.74 ± 0.11 %	$84.39 \pm 1.08 \pm 1.42$ %	0.962 ± 0.020

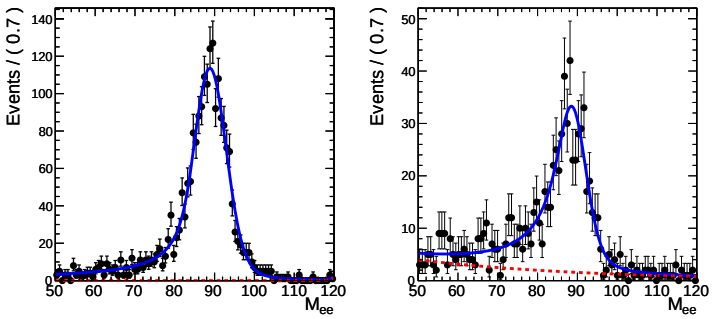

(a)

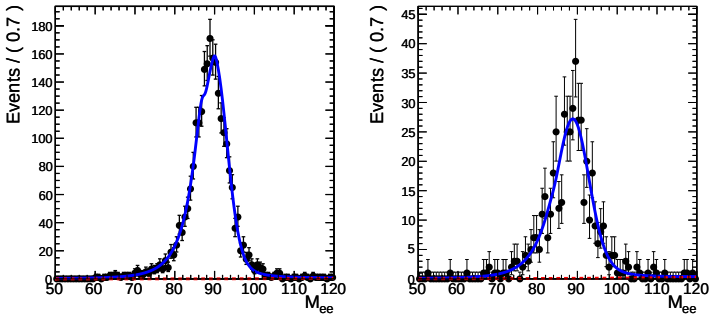

(b)

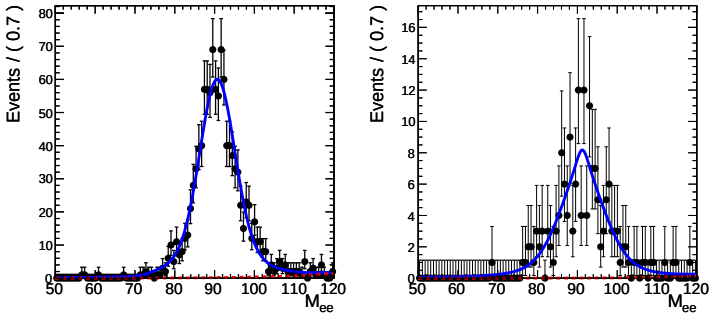

(c)

Figure 7: Fit to passing (left) and failing (right) data, (a) $20 < \mathrm{E_T} < 35$ (b) $35 < \mathrm{E_T} < 45$ (c) $\mathrm{E_T} > 45$.

Table 10: Hgg photon selection efficiency computed with fits method as a function of the photon R9 in barrel and endcap.

R9	**MC**	**DATA**	R (DATA/MC)
Barrel			
0 - 0.8	80.36 ± 0.09 %	$73.69 \pm 1.03 \pm 3.12$ %	0.917 ± 0.041
0.80 - 0.94	81.46 ± 0.09 %	$73.90 \pm 0.61 \pm 0.53$ %	0.907 ± 0.010
0.94 - 1.0	81.34 ± 0.09 %	$73.95 \pm 0.59 \pm 1.79$ %	0.909 ± 0.023
Endcap			
0 - 0.8	77.76 ± 0.20 %	$72.97 \pm 1.95 \pm 3.95$ %	0.938 ± 0.056
0.80 - 0.94	83.96 ± 0.11 %	$81.34 \pm 0.89 \pm 1.49$ %	0.969 ± 0.021
0.94 - 1.0	89.01 ± 0.11 %	$87.25 \pm 0.85 \pm 0.96$ %	0.980 ± 0.014

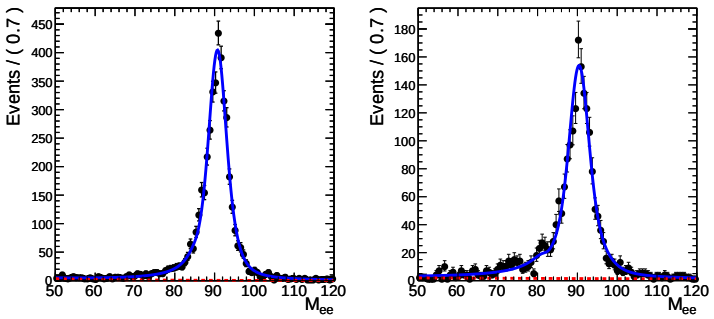

(a)

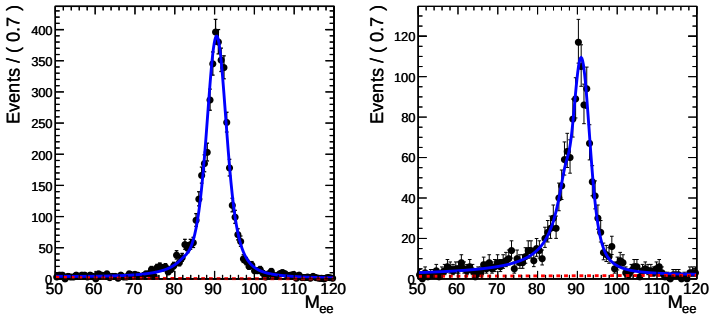

(b)

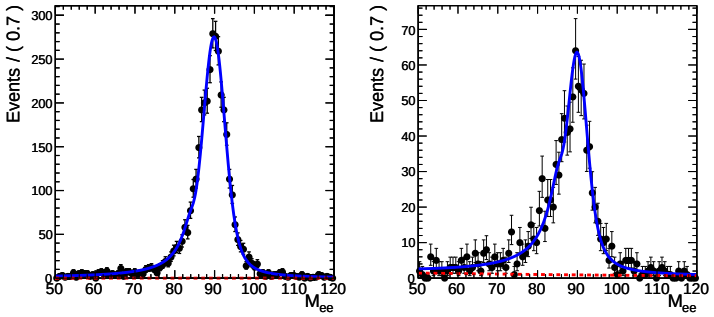

(c)

Figure 8: Fit to passing (left) and failing (right) data, (a) $0 < |\eta| < 0.5$ (b) $0.5 < |\eta| < 1.0$ (c) $|\eta| > 1.0$.

Table 11: Hgg photon selection efficiency computed with fits method as a function of the electron fBrem in barrel and endcap.

fBrem	**MC**	**DATA**	R (DATA/MC)
Barrel			
-0.2 - 0.2	78.35 ± 0.09 %	$69.05 \pm 0.93 \pm 1.97$ %	0.881 ± 0.028
0.2 - 0.6	82.14 ± 0.09 %	$74.73 \pm 0.75 \pm 1.07$ %	0.910 ± 0.016
0.6 - 1.0	83.00 ± 0.09 %	$77.75 \pm 0.71 \pm 1.32$ %	0.936 ± 0.018
Endcap			
-0.2 - 0.2	84.87 ± 0.19 %	$77.52 \pm 2.39 \pm 2.59$ %	0.913 ± 0.042
0.2 - 0.6	85.04 ± 0.12 %	$81.86 \pm 0.96 \pm 1.89$ %	0.962 ± 0.025
0.6 - 1.0	84.11 ± 0.12 %	$81.65 \pm 0.92 \pm 1.15$ %	0.971 ± 0.018

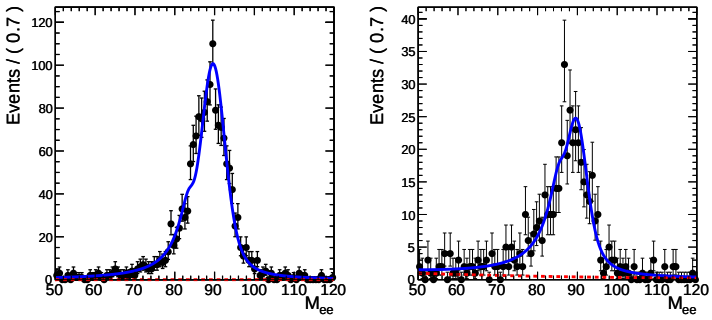

(a)

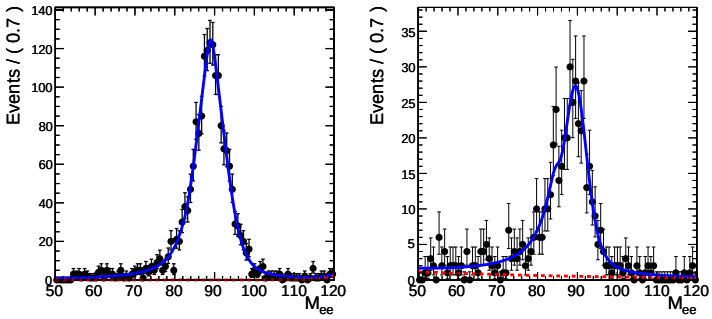

(b)

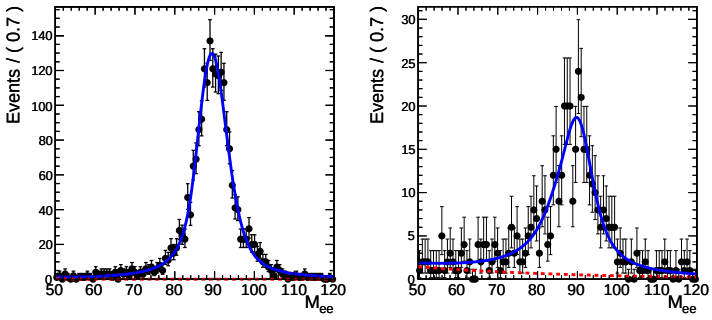

(c)

Figure 9: Fit to passing (left) and failing (right) data (blue line): (a) $1.566 < |\eta| < 1.8$ (b) $1.8 < |\eta| < 2.1$ (c) $|\eta| > 2.1$. The background contribution is also shown (red dashed line).

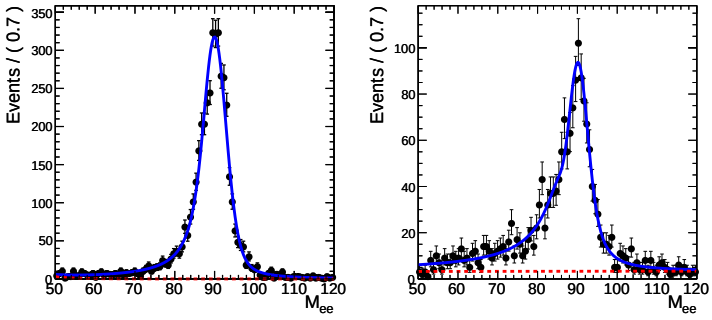

(a)

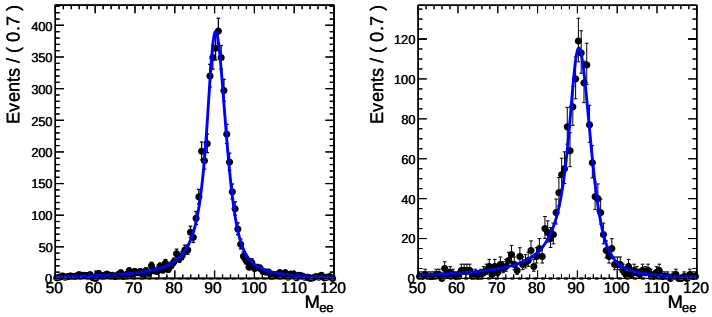

(b)

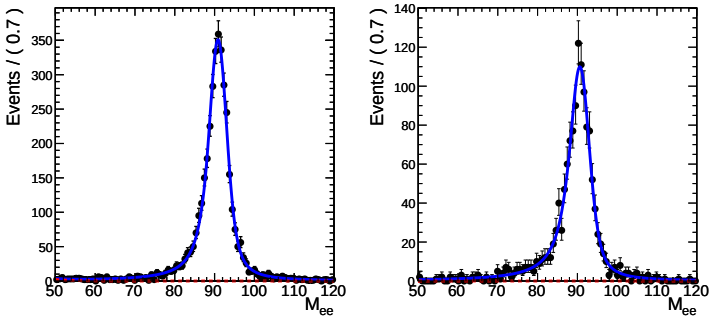

(c)

Figure 10: Fit to passing (left) and failing (right) data (blue line): (a) $0 < R9 < 0.8$ (b) $0.8 < R9 < 0.94$ (c) $R9 > 0.94$.

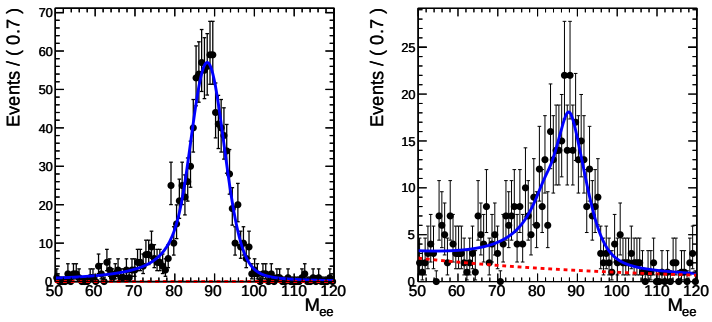

(a)

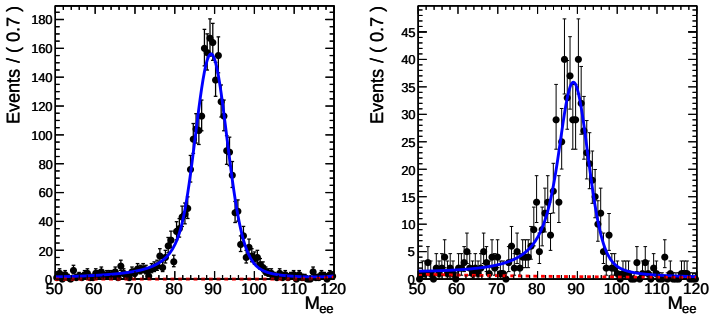

(b)

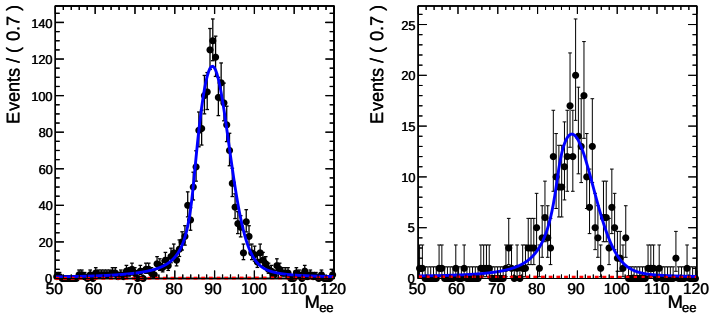

(c)

Figure 11: Fit to passing (left) and failing (right) data (blue line): (a) $0 < R9 < 0.8$ (b) $0.8 < R9 < 0.94$ (c) $R9 > 0.94$. The background contribution is also shown (red dashed line).

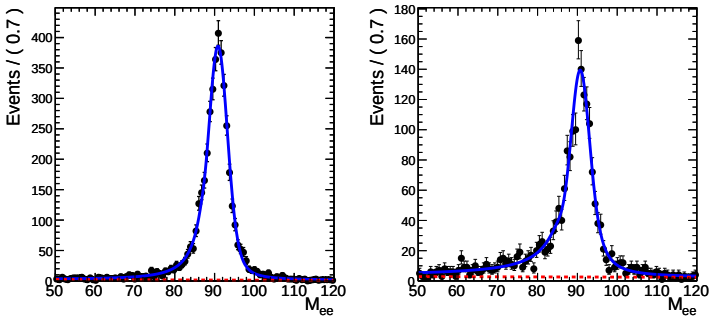

(a)

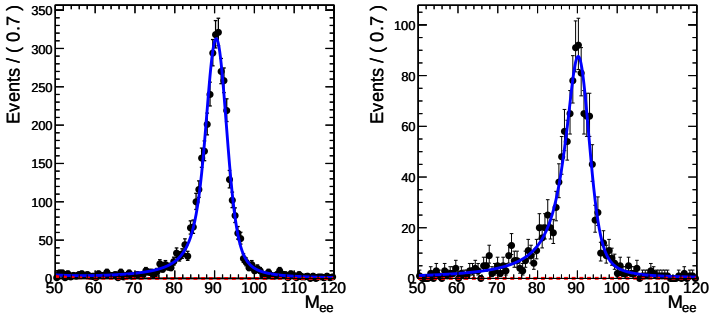

(b)

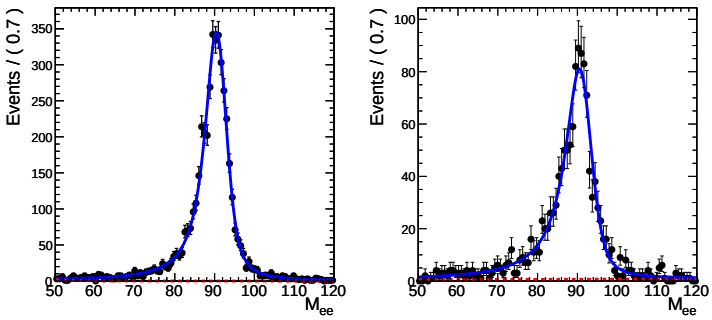

(c)

Figure 12: Fit to passing (left) and failing (right) data (blue line): (a) $-0.2 < fBrem < 0.2$ (b) $0.2 < fBrem < 0.6$ (c) $fBrem > 0.6$. The background contribution is also shown (red dashed line).

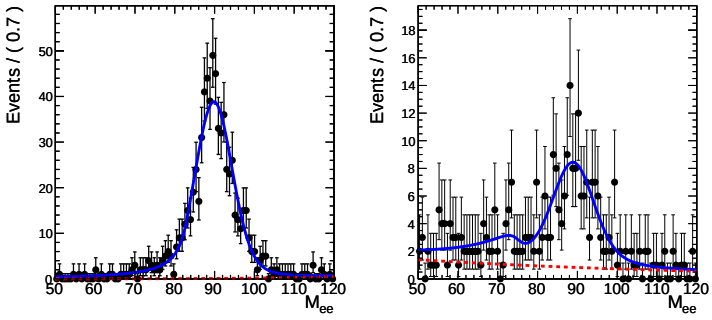

(a)

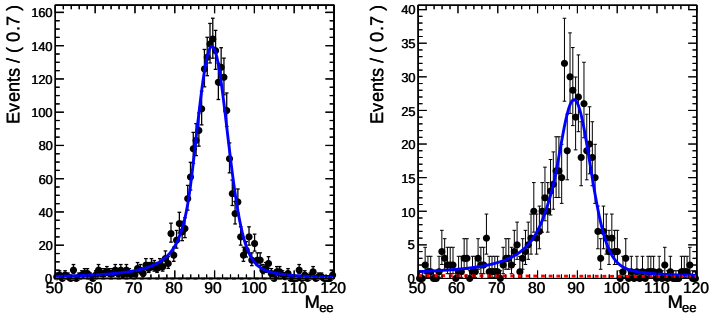

(b)

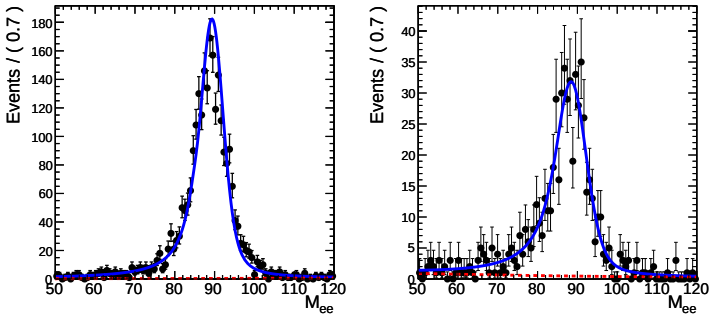

(c)

Figure 13: Fit to passing (left) and failing (right) data (blue line): (a) $-0.2 < fBrem < 0.2$ (b) $0.2 < fBrem < 0.6$ (c) $fBrem > 0.6$. The background contribution is also shown (red dashed line).

4.3 Opposite-Sign Same-Sign Method

As described in the previous section the number of signal events has been computed using Equation 1. The estimated charge mis-identification probabilities in passing and failing events used in this analysis and computed using Equation 2 are reported in Tables 12 and 13 .

The resulting efficiencies are instead shown in Tables 14 to 17 as a function of the probe E_T, η, R9 and fBrem.

The statistical error is assumed to be binomial. The systematic errors come from the uncertainty in the charge mis-identification and on the number of same-sign opposite-sign background events and they are computed assuming 50% uncertainty on the former and 100% on the latter contribution with the background contribution being the dominant one.

Table 12: Charge misidentification in barrel and endcap as a function of the electron E_T.

	Passing	**Failing**
Barrel		
20 - 35	0.56%	1.97%
35 - 45	0.54%	0.78%
45 - inf	0.44%	0.78%
Endcap		
20 - 35	1.88%	3.40%
35 - 45	2.30%	2.66%
45 - inf	2.53%	3.05%

Table 13: Charge misidentification in barrel and endcap as a function of the electron η.

	Passing	**Failing**
Barrel		
0 - 0.5	0.34%	0.98%
0.5 - 1.0	0.45%	1.25%
1.0 - 1.4442	0.81%	1.83%
TOT	0.52%	1.24%
Endcap		
1.566 - 1.8	1.87%	2.82%
1.8 - 2.1	2.00%	2.72%
2.1 - 2.5	2.67%	3.85%
TOT	2.21%	3.07%

Table 14: Hgg photon selection efficiency computed using opposite-same sign method as a function of the photon transverse energy in barrel and endcap.

ET	**MC**	**DATA**	R (DATA/MC)
Barrel			
20 - 35	$74.98 \pm 0.11\%$	$69.87 \pm 0.65 \pm 3.04\%$	0.935 ± 0.042
35 - 45	$82.43 \pm 0.08\%$	$76.67 \pm 0.49 \pm 0.68\%$	0.929 ± 0.010
45 - inf	$85.75 \pm 0.09\%$	$78.65 \pm 0.63 \pm 0.32\%$	0.917 ± 0.008
Endcap			
20 - 35	$79.46 \pm 0.14\%$	$78.20 \pm 0.79 \pm 3.47\%$	0.984 ± 0.045
35 - 45	$86.56 \pm 0.11\%$	$84.81 \pm 0.68 \pm 1.06\%$	0.979 ± 0.014
45 - inf	$90.04 \pm 0.14\%$	$87.67 \pm 0.94 \pm 0.43\%$	0.974 ± 0.011

Also in this case no factorization is involved and in future we will check if it can help in reducing the final uncertainty on the measurement.

Table 15: Hgg photon selection efficiency computed using opposite-same sign method as a function of the photon pseudorapidity in barrel and endcap.

η	**MC**	**DATA**	R (DATA/MC)
0 - 0.5	77.55 $\pm$ 0.09 %	70.18 $\pm$ 0.57 $\pm$ 1.63 %	0.905 $\pm$ 0.022
0.5 - 1.0	81.87 $\pm$ 0.09 %	76.47 $\pm$ 0.55 $\pm$ 1.24 %	0.934 $\pm$ 0.016
1.0 - 1.4442	84.69 $\pm$ 0.09 %	80.52 $\pm$ 0.58 $\pm$ 1.68 %	0.951 $\pm$ 0.021
1.566 - 1.8	83.34 $\pm$ 0.14 %	79.65 $\pm$ 0.89 $\pm$ 1.97 %	0.956 $\pm$ 0.026
1.8 - 2.1	82.38 $\pm$ 0.14 %	80.99 $\pm$ 0.82 $\pm$ 1.92 %	0.983 $\pm$ 0.025
2.1 - 2.5	87.74 $\pm$ 0.11 %	86.05 $\pm$ 0.70 $\pm$ 1.39 %	0.980 $\pm$ 0.017

Table 16: Hgg photon selection efficiency computed using opposite-same sign method as a function of the photon R9 in barrel and endcap.

R9	**MC**	**DATA**	R (DATA/MC)
Barrel			
0 - 0.8	80.36 $\pm$ 0.09 %	76.13 $\pm$ 0.57 $\pm$ 3.64 %	0.947 $\pm$ 0.046
0.80 - 0.94	81.46 $\pm$ 0.09 %	74.96 $\pm$ 0.55 $\pm$ 0.50 %	0.920 $\pm$ 0.009
0.94 - 1.0	81.34 $\pm$ 0.09 %	74.13 $\pm$ 0.62 $\pm$ 0.16 %	0.912 $\pm$ 0.007
Endcap			
0 - 0.8	77.76 $\pm$ 0.20 %	76.77 $\pm$ 1.14 $\pm$ 3.13 %	0.987 $\pm$ 0.043
0.80 - 0.94	83.96 $\pm$ 0.11 %	81.36 $\pm$ 0.68 $\pm$ 0.46 %	0.969 $\pm$ 0.009
0.94 - 1.0	89.01 $\pm$ 0.11 %	86.86 $\pm$ 0.72 $\pm$ 0.15 %	0.976 $\pm$ 0.009

Table 17: Hgg photon selection efficiency computed using opposite-same sign method as a function of the electron fBrem in barrel and endcap.

fBrem	**MC**	**DATA**	R (DATA/MC)
Barrel			
-0.2 - 0.2	78.35 $\pm$ 0.09 %	72.24 $\pm$ 0.58 $\pm$ 3.23 %	0.922 $\pm$ 0.042
0.2 - 0.6	82.14 $\pm$ 0.09 %	75.75 $\pm$ 0.60 $\pm$ 0.56 %	0.923 $\pm$ 0.010
0.6 - 1.0	83.00 $\pm$ 0.09 %	77.93 $\pm$ 0.55 $\pm$ 0.46 %	0.939 $\pm$ 0.009
Endcap			
-0.2 - 0.2	84.87 $\pm$ 0.19 %	82.02 $\pm$ 1.28 $\pm$ 3.86 %	0.966 $\pm$ 0.048
0.2 - 0.6	85.04 $\pm$ 0.12 %	82.11 $\pm$ 0.73 $\pm$ 0.36 %	0.965 $\pm$ 0.009
0.6 - 1.0	84.11 $\pm$ 0.12 %	82.52 $\pm$ 0.69 $\pm$ 0.98 %	0.981 $\pm$ 0.014

4.4 Pileup

During 2010 LHC operation the number of pileup events accompaning the primary interaction has largely changed from 0 up to an average of about 2 at the end of the data-taking.

Figure 14 is showing the distribution of the reconstructed vertices comparing data and the newly simulated samples.

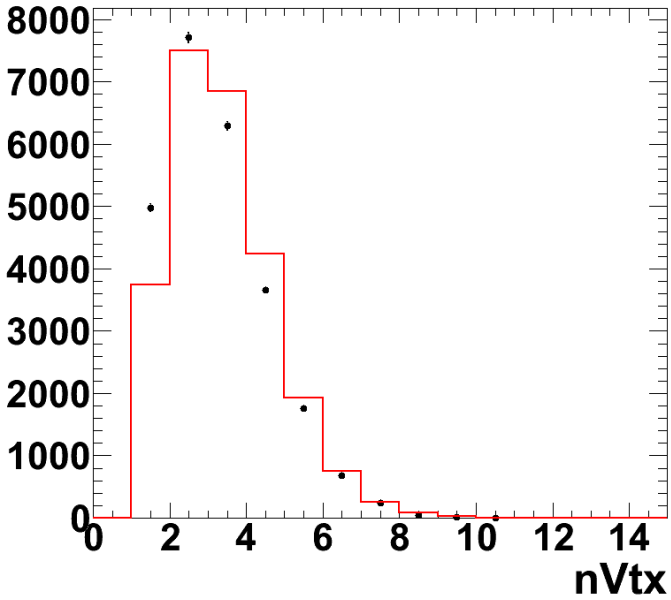

Figure 14: Number of reconstructed vertices in data (black dots) and MC (red line). MC events are normalized to the total integrated luminosity.

From the photon selection point of view the only affected variables are: ECAL and HCAL Isolation. Their distributions as a function of the number of vertices is shown in Figure 15. The Figure also shows Tracker Isolation which is not affected by pileup since only the tracks compatible with the electron vertex are considered in the p_T sum.

Figures 16, 17 and 18 shows the isolation MC distributions compared to data.

The ratio between Hgg Photon ID efficiency in MC without and with pileup is 1.053 in the barrel and 1.013 in the endcap. Table 18 reports the MC efficiencies as a function of the number of reconstructed vertices.

Table 18: Hgg photon selection efficiency as a function of the number of reconstructed vertices in signal MC.

N vtx	**Efficiency**
Barrel	
1	81.58 $\pm$ 0.27 %
2	79.83 $\pm$ 0.19 %
3	77.45 $\pm$ 0.21 %
>=4	73.76 $\pm$ 0.20 %
Endcap	
1	85.56 $\pm$ 0.36 %
2	84.73 $\pm$ 0.26 %
3	84.34 $\pm$ 0.27 %
>=4	82.49 $\pm$ 0.26 %

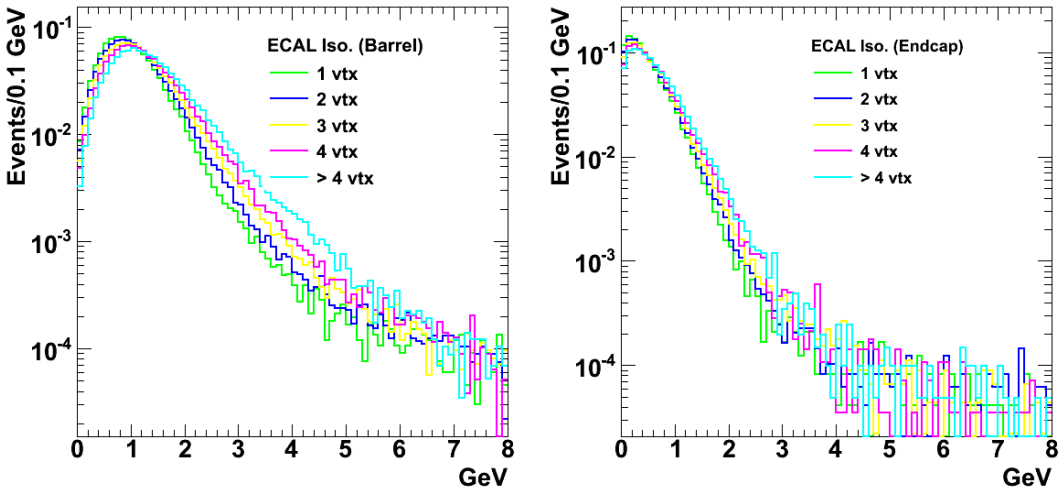

(a)

(b)

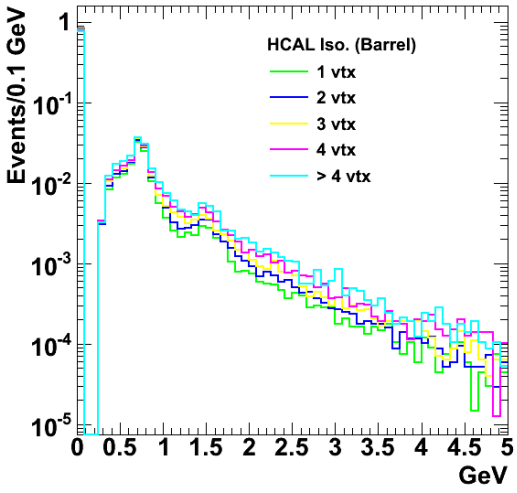

(c)

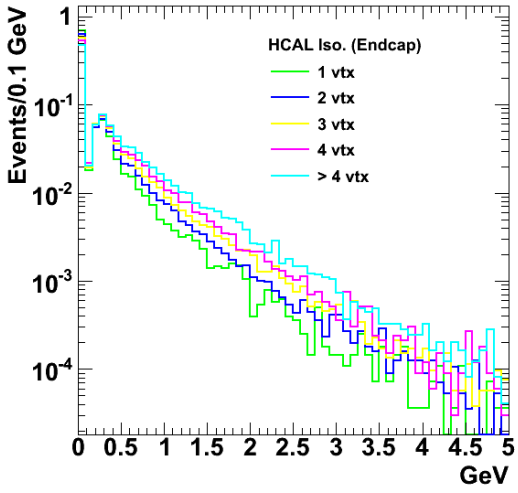

(d)

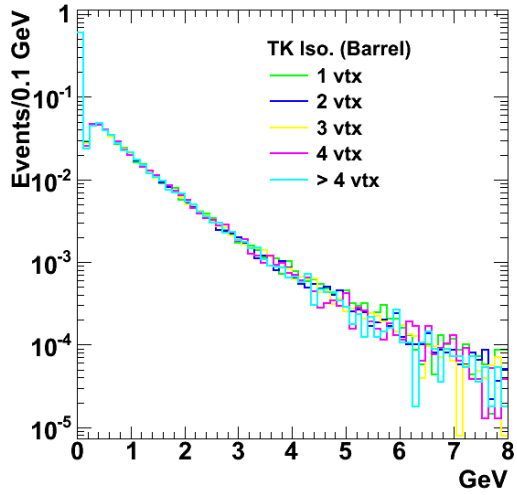

(e)

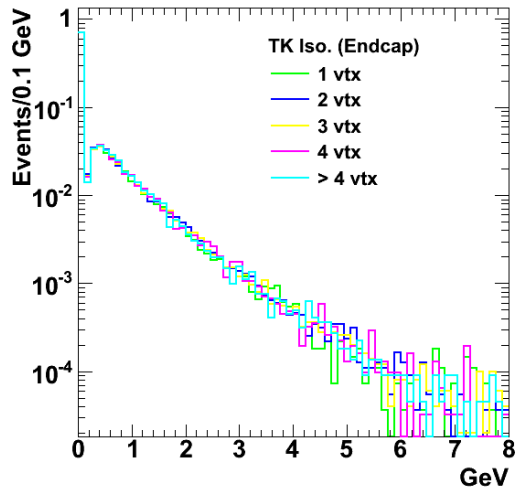

(f)

Figure 15: Isolation variables in barrel and endcap as a function of the number of reconstructed vertices: (a-b) ECAL, (c-d) HCAL and (e-f) Tracker.

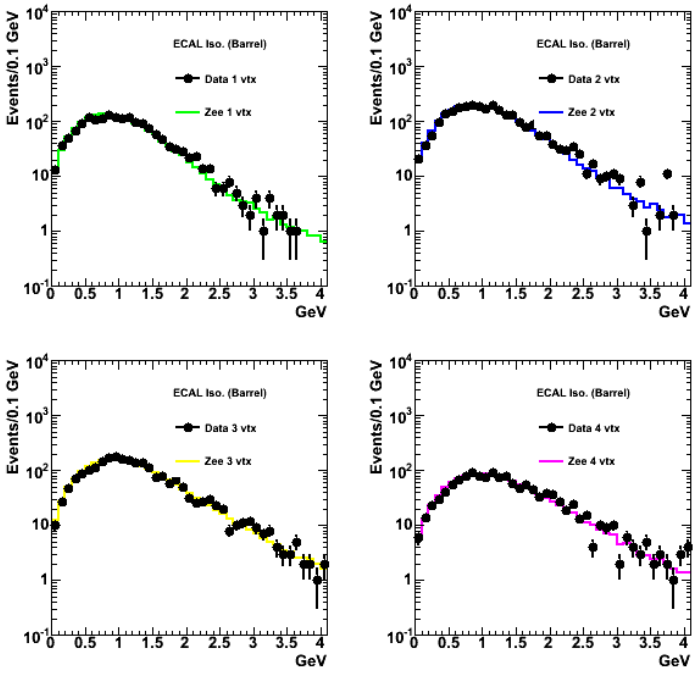

(a)

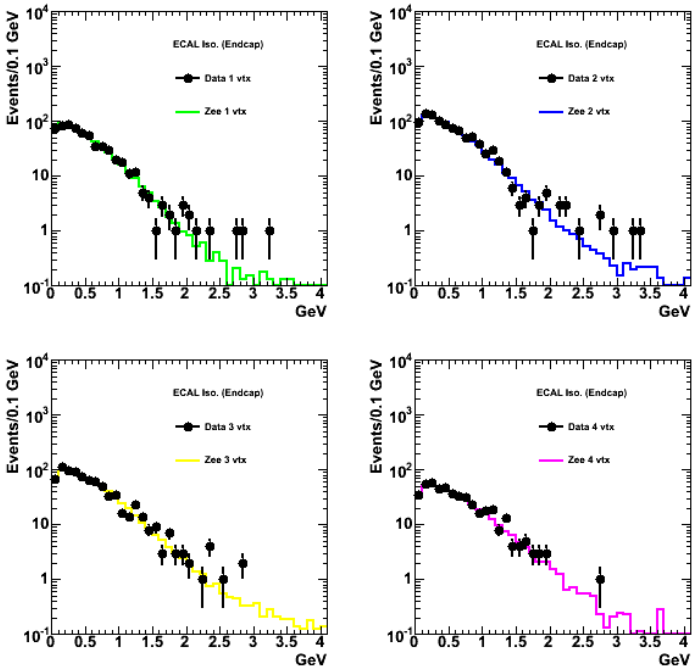

(b)

Figure 16: Data MC comparison of ECAL Isolation as a function of the number of reconstructed vertices.

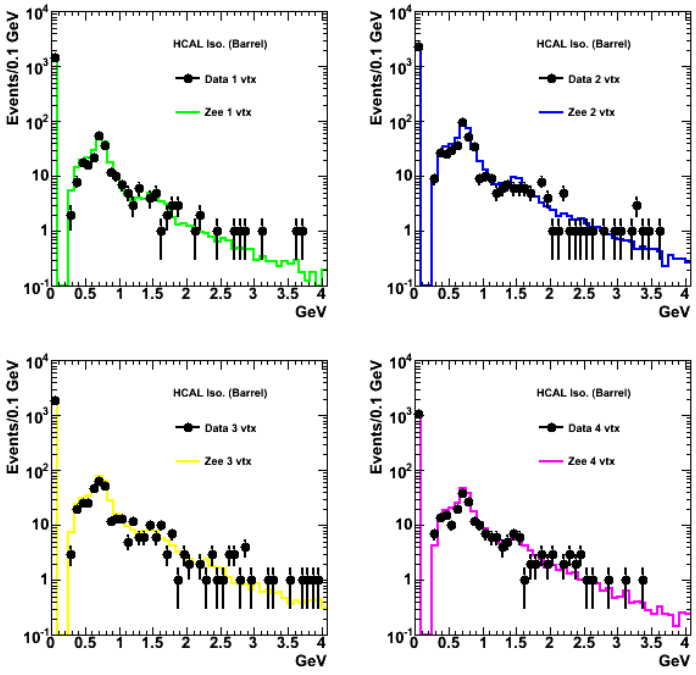

(a)

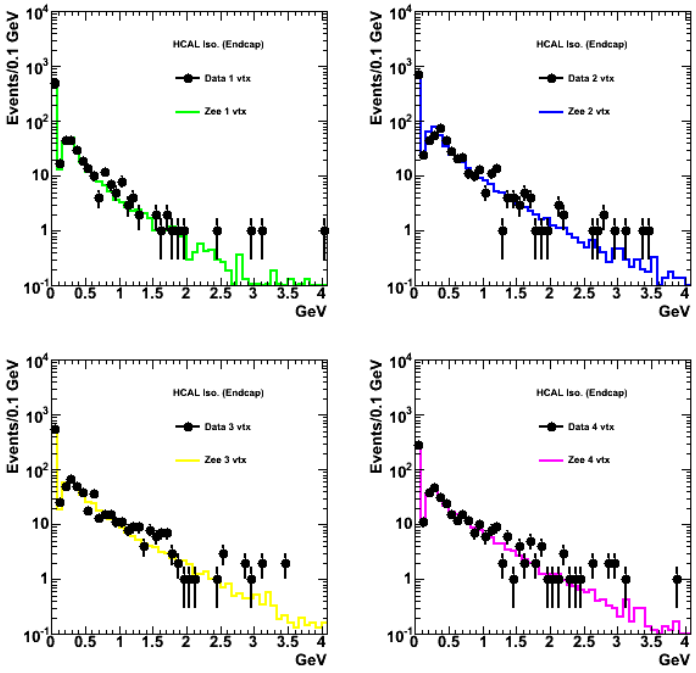

(b)

Figure 17: Data MC comparison of HCAL Isolation as a function of the number of reconstructed vertices.

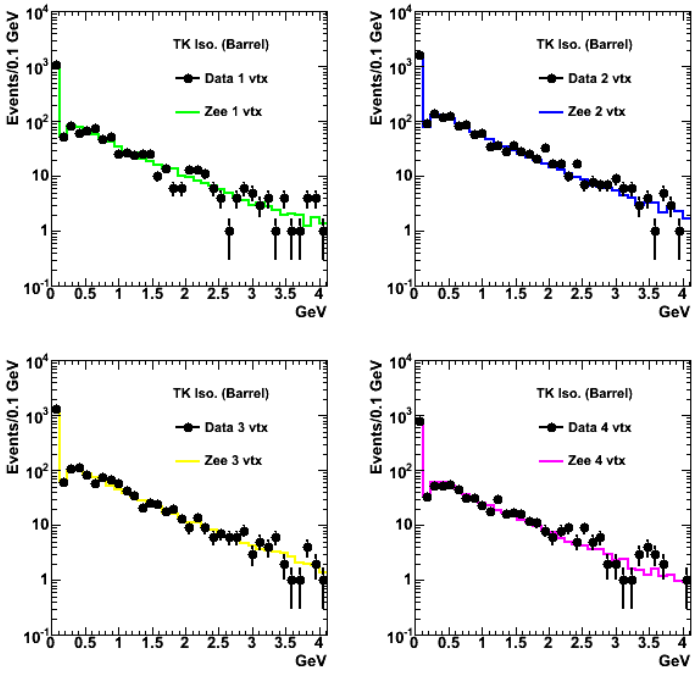

(a)

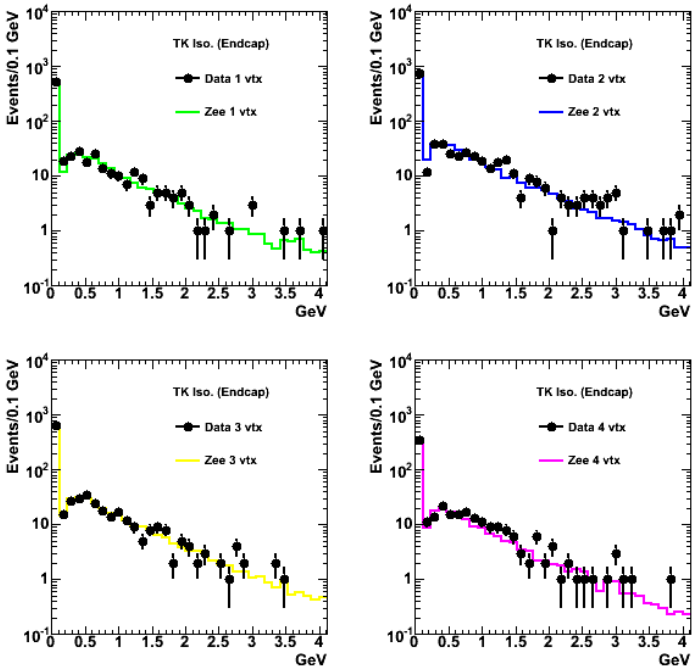

(b)

Figure 18: Data MC comparison of Tracker Isolation as a function of the number of reconstructed vertices.

5 Conclusions

We have performed a data-driven measurement of the efficiency of various photon identification selection using Z Tag and Probe method. Almost $35\mathrm{pb}^{-1}$ of data have been analyzed and the results have been presented as a function of different probe observables: E_T, η, R9, and fBrem. We have also checked the consistency of the results of three different methods: simple counting, fit and opposite-sign same-sign.

The results show that the three methods produce consistent results and efficiency in data is found to be lower than expected from MC. The main source of this discrepancy can be identified in the pileup which is not simulated in the currently used MC samples and which mainly affects calorimetric isolation variables. We have checked, comparing MC samples with and without pileup, that the selection is about 5% less efficient in the sample with pileup.

Previous studies done with less statistic ($3\mathrm{pb}^{-1}$) and with an older software release (CMSSW_3_6_X) showed that efficiency in data was to be $2-3\%$ higher than the efficiency measured in the MC, with the discrepancy coming predominantly from the tracker isolation cut.

A CMSSW_3_6_X Data and MC Samples

A.1 Data

The data used for this analysis consists of the 3.1 pb^{-1} included in runs up to 144114 collected in RunA during data-taking with the CMS detector at $\sqrt{s}$ = 7 TeV in 2010. The specific datasets used are defined in Table 19.

Table 19: Datasets used in this analysis.

Run Range	Dataset Name
132440 - 135802	/MinimumBias/Commissioning10-SD_EG-Jun14thSkim_v1/ RECO
135803 - 137632	/EG/Run2010A-Jun14thReReco_v1/RECO
137633 - 139777	/EG/Run2010A-PromptReco-v4/RECO
139778 - 140160	/EG/Run2010A-Jul16thReReco-v2/RECO
140161 - 144144	/EG/Run2010A-PromptReco-v4/RECO

The official PromptReco JSON file, Cert_132440-144114_7TeV_StreamExpress_Collisions10_JSON.txt, was used to select good lumi sections from these runs.

A.2 Monte Carlo

Monte Carlo samples from the Summer10 CMSSW_3_7_X re digitization were used. The signals and backgrounds were all generated with PYTHIA [2]. Table 20 shows the samples and equivalent integrated luminosities used. Two γ+Jet samples were used: a sample with $\hat{p_t}$ greater than 15 GeV/c and one with 30 GeV/c. For the $\hat{p_t}$ 15 GeV/$c$sample all events with a $\hat{p_t}$ of 30 GeV/c or above were removed to avoid double counting. All cross sections used are LO PYTHIA cross sections except the $Z/\gamma* \rightarrow ee$ signal sample for which the NLO k-factor, 1.2275, was applied.

Table 20: List of Monte Carlo samples used in the analysis. The corresponding integrated luminosity is also reported.

Process	$\hat{p_t}$ range (GeV/c)	$\int Ldt$ (pb^{-1})
Z/$\gamma*$ $\rightarrow$ee (Signal)		125.3
W $\rightarrow$eν		26.5
γ + Jet	> 15	6.2
γ + Jet	> 30	42.2
QCD bc$\rightarrow$e	$20 - 30$	8.7
QCD bc$\rightarrow$e	$30 - 80$	6.7
QCD bc$\rightarrow$e	$80 - 170$	106.1
QCD EM Enriched	$20 - 30$	13.1
QCD EM Enriched	$30 - 80$	11.3
QCD EM Enriched	$80 - 170$	38.3

B CMSSW_3_6_X Photon ID

B.1 Loose Selection

Tables 21 and 22 show the loose selection efficiency as a function of the photon E_T in the barrel and endcap. The uncertainty quoted for the data results is the combination of the binomial statistical error and the systematic error (estimated to be 100% of the background from MC). The table also shows the corresponding MC efficiency computed on Z electrons and the ratio of the efficiency for photons (measured on MC γ+Jet events) and electrons (measured on Z electrons).

All the results have been corrected to take into account possible correlations between the two sets of cuts. Correlations are estimated as the difference between the direct and factorized loose selection efficiency computed on MC (about 1.5%).

A discrepancy between the efficiency from MC and data is seen. Looking at the individual efficiencies of each

Table 21: Loose photon selection efficiency as a function of the photon transverse energy in the barrel. The MC efficiency (measured on electrons) and the ratio between MC efficiencies estimated for photons and electrons are also shown.

ET	MC	DATA	MC Ratio γ/e
20 - 35	$84.18 \pm 0.20\%$	$86.73 \pm 1.69\%$	1.032 ± 0.003
35 - 45	$87.27 \pm 0.19\%$	$89.28 \pm 1.27\%$	1.025 ± 0.004
45 - inf	$88.50 \pm 0.23\%$	$89.04 \pm 1.83\%$	1.005 ± 0.005
TOT	$86.30 \pm 0.12\%$	$88.41 \pm 0.89\%$	1.012 ± 0.002

Table 22: Loose photon selection efficiency as a function of the photon transverse energy in the endcap. The MC efficiency (measured on electrons) and the ratio between MC efficiencies estimated for photons and electrons are also shown.

ET	MC	DATA	MC Ratio γ/e
20 - 35	$87.40 \pm 0.25\%$	$92.24 \pm 2.70\%$	1.035 ± 0.003
35 - 45	$91.33 \pm 0.22\%$	$91.43 \pm 2.43\%$	1.008 ± 0.005
45 - inf	$92.55 \pm 0.26\%$	$91.06 \pm 3.23\%$	1.013 ± 0.005
TOT	$90.05 \pm 0.14\%$	$91.59 \pm 1.60\%$	1.009 ± 0.002

cut, the discrepancy can be seen to come primarily from the tracker isolation. Computing the efficiency for tracker isolation using the reconstructed electron isolation variable shows the same discrepancy.

Figure 19 shows the electron invariant mass distributions for events passing (left) and failing (right) the isolation cuts of the loose photon selection. The contribution of the different channels estimated from MC is also shown.

The loose photon selection efficiency as a function of η, R9 and fBrem are reported in the following.

B.2 Tight Selection

Tables 26 and 27 show the tight selection efficiencies as a function of the photon E_T in the barrel and endcap. As for the loose efficiencies, the quoted numbers have been corrected to take into account possible correlations between the two sets of cuts. Correlations are estimated to be about 2.5%.

Figure 20 shows the electron invariant mass distributions for events passing (left) and failing (right) the isolation cuts of the loose photon selection. The contribution of the different channels estimated from MC is also shown.

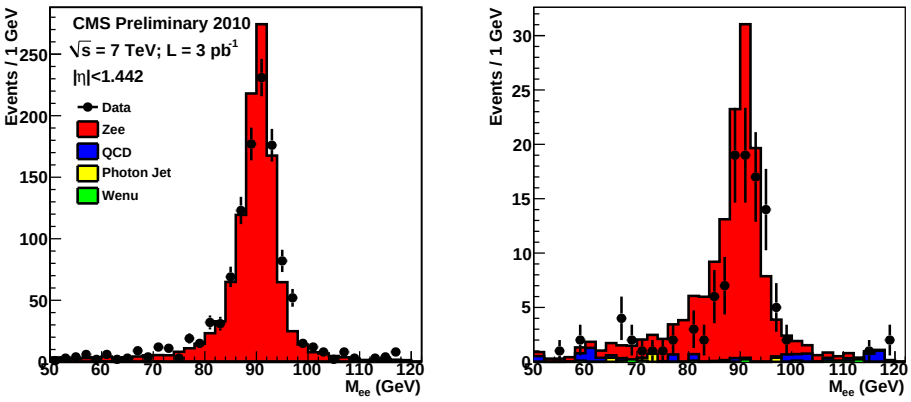

Figure 19: Electron invariant mass distribution for events passing (left) and failing (right) isolation cuts of the loose photon selection in the barrel. The contribution of the different channels estimated from MC is also shown. MC events are normalized to the total integrated luminosity used in this analysis.

Table 23: Loose selection efficiency in barrel and endcap as a function of photon η.

ETA	**MC**	**DATA**
0 - 0.5	85.12%	87.97% $\pm$ 1.44%
0.5 - 1.0	86.22%	87.31% $\pm$ 1.52%
1.0 - 1.442	87.87%	89.42% $\pm$ 1.64%
TOT	86.30%	88.15% $\pm$ 0.88%
1.56 - 1.8	88.37%	89.29% $\pm$ 2.82%
1.8 - 2.1	88.87%	88.54% $\pm$ 3.30%
2.1 - 2.5	92.24%	96.90% $\pm$ 1.50%
TOT	90.05%	91.37% $\pm$ 1.63%

Table 24: Loose selection efficiency in barrel and endcap as a function of photon R9.

	Barrel		Endcap	
R9	**MC**	**DATA**	**MC**	**DATA**
0 - 0.8	85.46%	88.34% $\pm$ 1.48%	85.01%	81.62% $\pm$ 5.69%
0.8 - 0.94	86.15%	87.07% $\pm$ 1.63%	89.42%	92.43% $\pm$ 2.20%
0.94 - 1.0	87.44%	88.83% $\pm$ 1.50%	93.30%	94.50% $\pm$ 2.38%
TOT	86.30%	88.09% $\pm$ 0.89%	90.05%	91.30% $\pm$ 1.62%

Table 25: Loose selection efficiency in barrel and endcap as a function of electron fBrem.

	Barrel		Endcap	
fBrem	**MC**	**DATA**	**MC**	**DATA**
-0.2 - 0.2	85.20%	88.94% $\pm$ 1.43%	90.92%	91.17% $\pm$ 3.92%
0.2 - 0.6	86.73%	86.75% $\pm$ 1.61%	90.31%	90.37% $\pm$ 2.71%
0.6 - 1.0	87.06%	88.83% $\pm$ 1.54%	89.45%	94.46% $\pm$ 1.41%
TOT	86.30%	88.14% $\pm$ 0.88%	90.05%	91.40% $\pm$ 1.62%

Table 26: Tight photon selection efficiency as a function of the photon transverse energy in the barrel. The MC efficiency (measured on electrons) and the ratio between MC efficiencies estimated for photons and electrons are also shown.

ET	**MC**	**Data**	**MC Ratio γ/e**
20 - 35	69.38 $\pm$ 0.18%	69.58 $\pm$ 2.80%	1.060 $\pm$ 0.004
35 - 45	72.78 $\pm$ 0.18%	71.94 $\pm$ 2.09%	1.047 $\pm$ 0.007
45 - inf	74.93 $\pm$ 0.22%	72.48 $\pm$ 2.92%	0.995 $\pm$ 0.008
TOT	71.90 $\pm$ 0.11%	71.31 $\pm$ 1.47%	1.028 $\pm$ 0.003

Table 27: Tight photon selection efficiency as a function of the photon transverse energy in the endcap. The MC efficiency (measured on electrons) and the ratio between MC efficiencies estimated for photons and electrons are also shown.

ET	MC	Data	MC Ratio γ/e
20 - 35	$71.30 \pm 0.28\%$	$71.07 \pm 3.94\%$	1.074 ± 0.006
35 - 45	$77.63 \pm 0.24\%$	$75.19 \pm 3.34\%$	1.028 ± 0.008
45 - inf	$80.87 \pm 0.31\%$	$73.48 \pm 4.98\%$	1.006 ± 0.009
TOT	$75.85 \pm 0.15\%$	$73.31 \pm 2.31\%$	1.019 ± 0.004

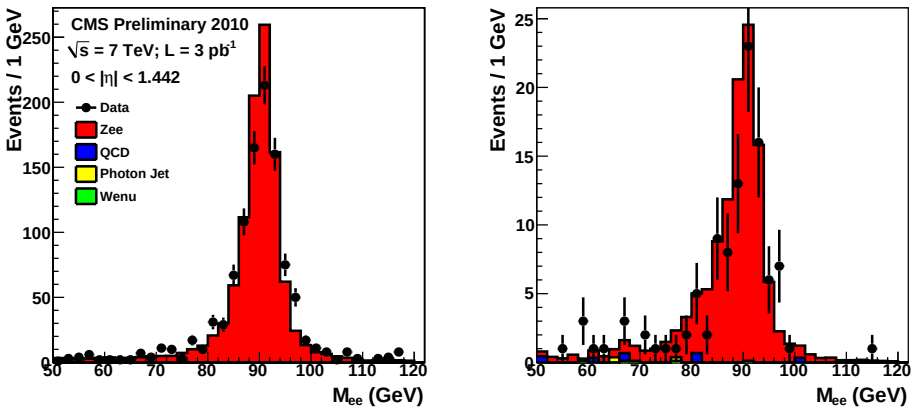

Figure 20: Electron invariant mass distribution for events passing (left) and failing (right) $\sigma_{i\eta i\eta}$ and H/E cuts of the tight photon selection in the barrel. The contribution of the different channels estimated from MC is also shown. MC events are normalized to the total integrated luminosity used in this analysis.

229 The tight photon selection efficiency as a function of η, R9 and fBrem are reported in the following.

Table 28: Tight selection efficiency in barrel and endcap as a function of photon η.

ETA	**MC**	**DATA**
0 - 0.5	69.35%	71.44% $\pm$ 2.39%
0.5 - 1.0	72.39%	68.80% $\pm$ 2.49%
1.0 - 1.442	74.47%	74.66% $\pm$ 2.53%
TOT	71.90%	71.37% $\pm$ 1.47%
1.56 - 1.8	72.54%	65.80% $\pm$ 4.49%
1.8 - 2.1	72.67%	71.69% $\pm$ 4.12%
2.1 - 2.5	81.01%	81.19% $\pm$ 3.06%
TOT	75.85%	73.63% $\pm$ 2.29%

Table 29: Tight selection efficiency in barrel and endcap as a function of photon R9.

	Barrel		Endcap	
R9	**MC**	**DATA**	**MC**	**DATA**
0 - 0.8	71.44%	74.30% $\pm$ 2.36%	68.01%	68.81% $\pm$ 5.55%
0.8 - 0.94	71.73%	67.16% $\pm$ 2.59%	75.07%	71.59% $\pm$ 3.35%
0.94 - 1.0	72.64%	73.05% $\pm$ 2.61%	81.46%	79.11% $\pm$ 3.51%
TOT	71.90%	71.39% $\pm$ 1.47%	76.14%	73.60% $\pm$ 2.30%

Table 30: Tight selection efficiency in barrel and endcap as a function of electron fBrem.

	Barrel		Endcap	
fBrem	**MC**	**DATA**	**MC**	**DATA**
-0.2 - 0.2	70.58%	69.88% $\pm$ 2.64%	78.25%	73.91% $\pm$ 6.51%
0.2 - 0.6	72.18%	71.35% $\pm$ 2.54%	76.65%	72.44% $\pm$ 3.69%
0.6 - 1.0	73.02%	72.60% $\pm$ 2.36%	74.82%	74.80% $\pm$ 3.17%
TOT	71.90%	71.28% $\pm$ 1.47%	76.14%	73.81% $\pm$ 2.31%

B.3 Pixel-Match Efficiency

Table 31 reports the resulting efficiencies.

Table 31: Pixel-Match efficiency measured in barrel and endcap using tag and probe technique. The corresponding MC estimate is also shown.

	MC	DATA	Stat	Syst	Tot
Barrel	98.79%	97.92%	0.41%	0.51%	0.65%
Endcap	97.06%	95.09%	1.27%	1.57%	2.02%

C Exotica Selection Efficiencies

C.1 Counting Method

Figure 21 shows the electron invariant mass distributions for events passing (left) and failing (right) the isolation cuts of the Exotica Photon ID selection. The contribution of the different channels estimated from MC is also shown. In this case the Dec22ReReco dataset has been used.

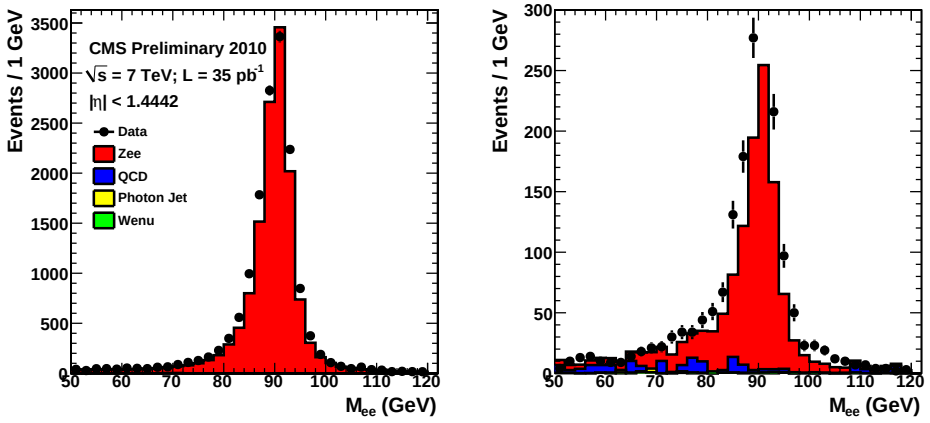

(a)

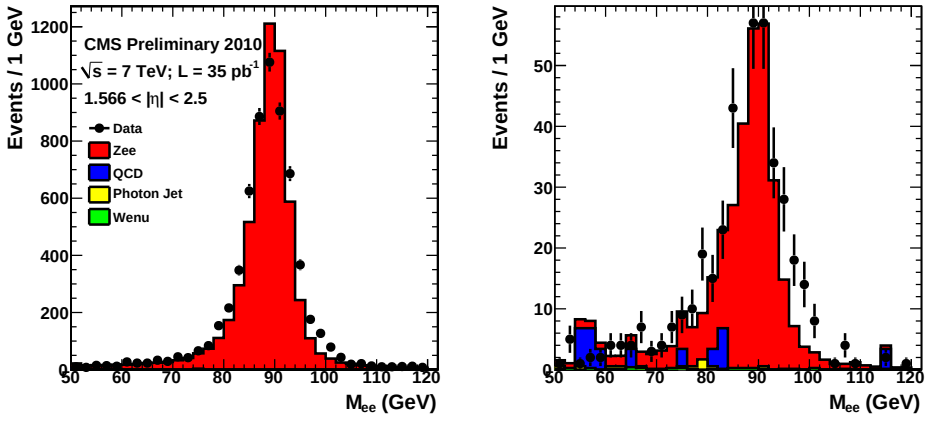

(b)

Figure 21: Electron invariant mass distribution for events passing (left) and failing (right) isolation cuts of the Exotica Photon ID selection in barrel (top) and endcap (bottom). The contribution of the different channels estimated from MC is also shown. MC events are normalized to the total integrated luminosity used in this analysis.

The Exotica selection efficiency has been also checked on MC photons using γ plus jet events. It turns out that the MC Ratio γ/e is about 1.01 in barrel and 1.001 in endcap.

Table 32: Exotica selection efficiency in barrel and endcap computed with the counting method as a function of photon $\mathrm{E_T}$.

$\mathrm{E_T}$	**MC**	**DATA**	R (DATA/MC)
Barrel			
20 - 35	86.97 $\pm$ 0.16 %	86.49 $\pm$ 0.45 $\pm$ 1.95 %	0.995 $\pm$ 0.023
35 - 45	92.21 $\pm$ 0.11 %	90.05 $\pm$ 0.33 $\pm$ 0.16 %	0.977 $\pm$ 0.004
45 - inf	93.61 $\pm$ 0.13 %	90.98 $\pm$ 0.43 $\pm$ 0.02 %	0.972 $\pm$ 0.005
Endcap			
20 - 35	88.54 $\pm$ 0.22 %	88.28 $\pm$ 0.55 $\pm$ 1.07 %	0.997 $\pm$ 0.014
35 - 45	93.20 $\pm$ 0.16 %	92.36 $\pm$ 0.49 $\pm$ 0.35 %	0.991 $\pm$ 0.007
45 - inf	94.94 $\pm$ 0.20 %	94.18 $\pm$ 0.62 $\pm$ 0.16 %	0.992 $\pm$ 0.007

Table 33: Exotica selection efficiency computed with the counting method as a function of photon η.

η	**MC**	**DATA**	R (DATA/MC)
0 - 0.5	90.63 $\pm$ 0.13 %	88.06 $\pm$ 0.38 $\pm$ 0.54 %	0.972 $\pm$ 0.008
0.5 - 1.0	91.02 $\pm$ 0.13 %	89.58 $\pm$ 0.38 $\pm$ 0.62 %	0.984 $\pm$ 0.008
1.0 - 1.4442	91.47 $\pm$ 0.14 %	90.64 $\pm$ 0.41 $\pm$ 0.88 %	0.991 $\pm$ 0.011
1.566 - 1.8	90.69 $\pm$ 0.21 %	88.98 $\pm$ 0.66 $\pm$ 0.33 %	0.981 $\pm$ 0.008
1.8 - 2.1	91.15 $\pm$ 0.20 %	90.95 $\pm$ 0.54 $\pm$ 0.35 %	0.998 $\pm$ 0.007
2.1 - 2.5	93.51 $\pm$ 0.17 %	92.63 $\pm$ 0.48 $\pm$ 0.94 %	0.990 $\pm$ 0.012

Table 34: Exotica selection efficiency in barrel and endcap computed with the counting method as a function of photon R9.

R9	**MC**	**DATA**	R (DATA/MC)
Barrel			
0 - 0.80	89.47 $\pm$ 0.15 %	88.31 $\pm$ 0.39 $\pm$ 1.55 %	0.987 $\pm$ 0.018
0.80 - 0.94	91.12 $\pm$ 0.13 %	89.48 $\pm$ 0.38 $\pm$ 0.36 %	0.982 $\pm$ 0.006
0.94 - 1.0	92.47 $\pm$ 0.14 %	90.11 $\pm$ 0.42 $\pm$ 0.08 %	0.975 $\pm$ 0.005
Endcap			
0 - 0.80	86.78 $\pm$ 0.33 %	86.14 $\pm$ 0.78 $\pm$ 1.65 %	0.993 $\pm$ 0.021
0.80 - 0.94	91.76 $\pm$ 0.17 %	91.13 $\pm$ 0.49 $\pm$ 0.53 %	0.993 $\pm$ 0.008
0.94 - 1.0	94.68 $\pm$ 0.16 %	93.73 $\pm$ 0.51 $\pm$ 0.03 %	0.990 $\pm$ 0.006

Table 35: Exotica selection efficiency in barrel and endcap computed with the counting method as a function of photon $\mathrm{E}/\mathrm{fbrem}$.

fBrem	**MC**	**DATA**	R (DATA/MC)
	Barrel		
-0.2 - 0.2	90.34 $\pm$ 0.13 %	88.69 $\pm$ 0.37 $\pm$ 1.30 %	0.981 $\pm$ 0.015
0.2 - 0.6	91.34 $\pm$ 0.14 %	89.47 $\pm$ 0.42 $\pm$ 0.30 %	0.979 $\pm$ 0.006
0.6 - 1.0	91.42 $\pm$ 0.13 %	89.94 $\pm$ 0.39 $\pm$ 0.30 %	0.984 $\pm$ 0.006
	Endcap		
-0.2 - 0.2	91.48 $\pm$ 0.30 %	89.69 $\pm$ 0.84 $\pm$ 2.07 %	0.980 $\pm$ 0.024
0.2 - 0.6	92.26 $\pm$ 0.17 %	91.83 $\pm$ 0.51 $\pm$ 0.43 %	0.995 $\pm$ 0.007
0.6 - 1.0	91.67 $\pm$ 0.18 %	90.57 $\pm$ 0.49 $\pm$ 0.14 %	0.988 $\pm$ 0.006

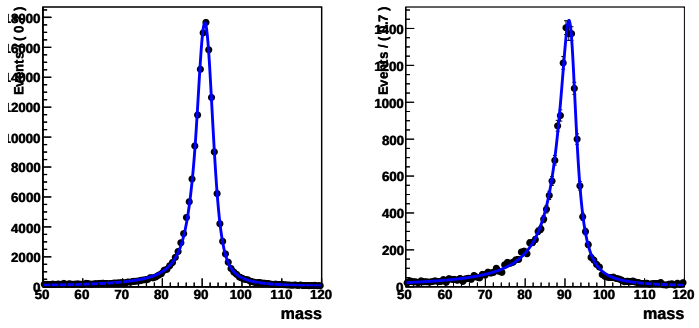

(a)

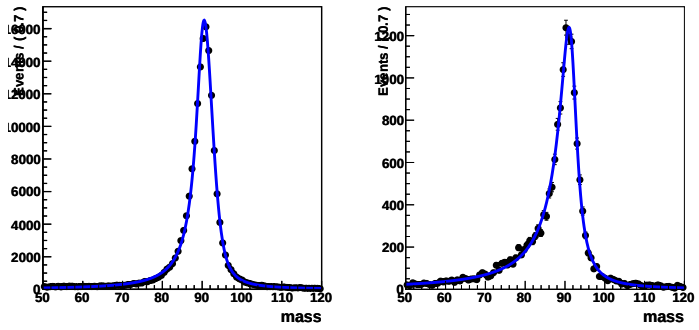

(b)

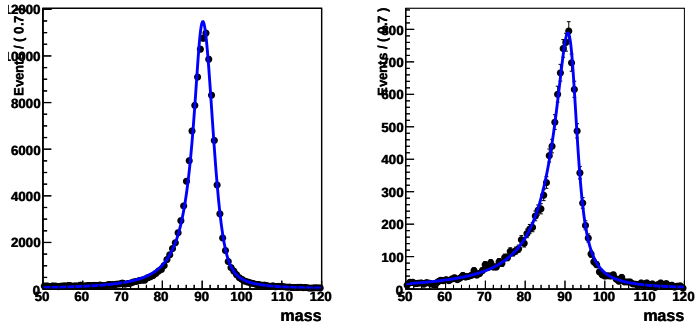

(c)

Figure 22: Fit to Z MC passing (left) and failing (right) distributions: (a) $0 < |\eta| < 0.5$ (d) $0.5 < |\eta| < 1.0$ (c) $|\eta| > 1.0$. The blue line represent Breit Wigner convoluted with the modified Crystal-Ball function resulting from the fit.

C.2 Fit Method

Figures 22 and 23 show example of fits to MC distribution.

Figures 24 and 25 show the fit results.

C.3 Opposite Sign Same Sign

C.4 Pileup

The ratio between Exotica Photon ID efficiency in MC without and with pileup is 1.008 in the barrel and 1.001 in the endcap. Table 44 reports the MC efficiencies as a function of the number of reconstructed vertices.

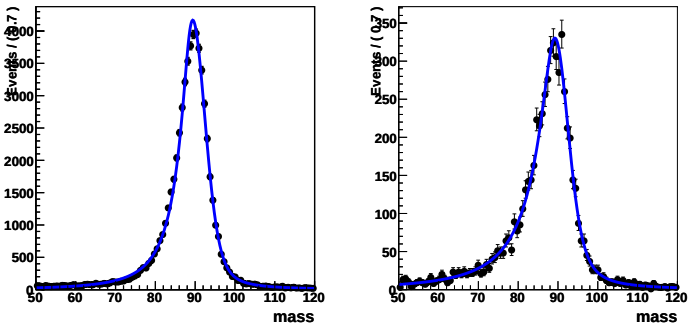

(a)

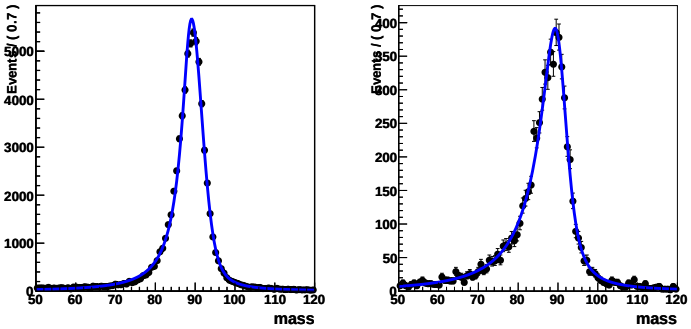

(b)

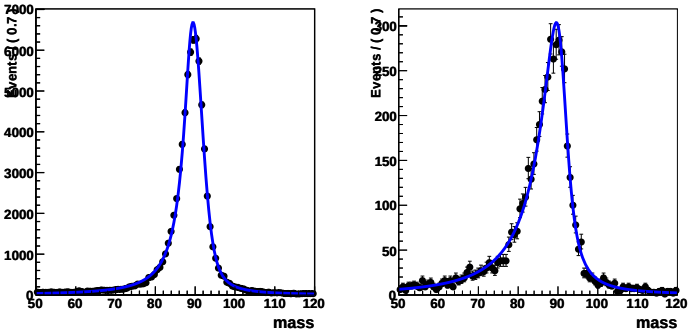

(c)

Figure 23: Fit to Z MC passing (left) and failing (right) distributions: (a) $1.566 < |\eta| < 1.8$ (b) $1.8 < |\eta| < 2.1$ (c) $|\eta| > 2.1$. The blue line represent Breit Wigner convoluted with the modified Crystal-Ball function resulting from the fit.

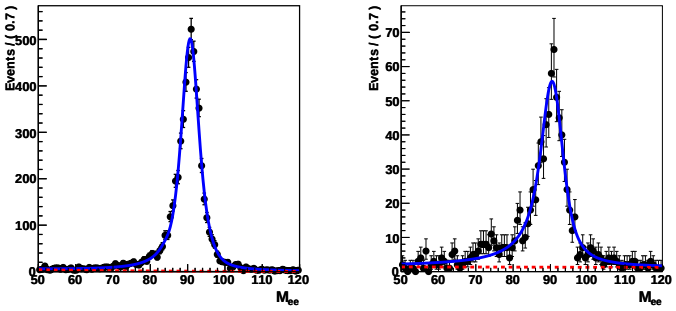

(a)

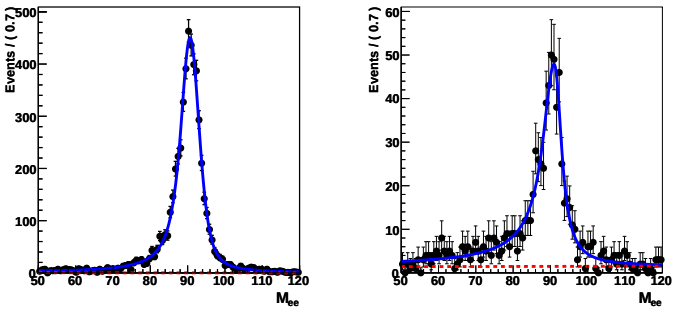

(b)

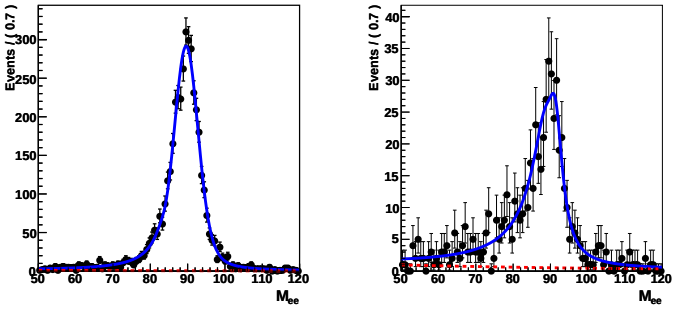

(c)

Figure 24: Fit to passing (left) and failing (right) data, (a) $0 < |\eta| < 0.5$ (b) $0.5 < |\eta| < 1.0$ (c) $|\eta| > 1.0$.

Table 36: Exotica selection efficiency in barrel and endcap computed with the fit method as a function of photon E_T.

E_T	**MC**	**DATA**	R (DATA/MC)
Barrel			
20 - 35	86.97 $\pm$ 0.16 %	82.23 $\pm$ 1.14 $\pm$ 1.58 %	0.945 $\pm$ 0.022
35 - 45	92.21 $\pm$ 0.11 %	89.54 $\pm$ 0.43 $\pm$ 0.55 %	0.971 $\pm$ 0.008
45 - inf	93.61 $\pm$ 0.13 %	90.77 $\pm$ 0.52 $\pm$ 0.82 %	0.970 $\pm$ 0.010
Endcap			
20 - 35	88.54 $\pm$ 0.22 %	88.89 $\pm$ 1.60 $\pm$ 3.44 %	1.004 $\pm$ 0.043
35 - 45	93.20 $\pm$ 0.16 %	90.99 $\pm$ 0.56 $\pm$ 0.43 %	0.977 $\pm$ 0.008
45 - inf	94.94 $\pm$ 0.20 %	93.42 $\pm$ 0.10 $\pm$ 0.95 %	0.984 $\pm$ 0.010

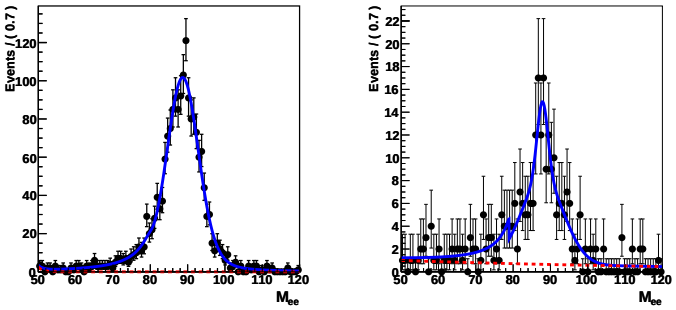

(a)

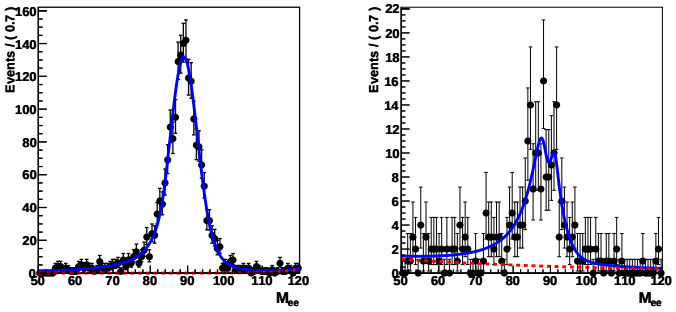

(b)

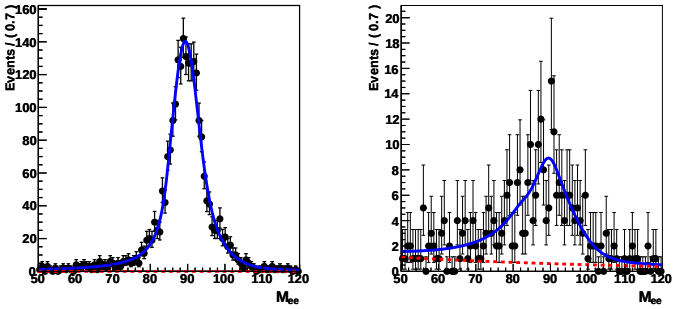

(c)

Figure 25: Fit to passing (left) and failing (right) data (blue line): (a) $1.566 < |\eta| < 1.8$ (b) $1.8 < |\eta| < 2.1$ (c) $|\eta| > 2.1$. The background contribution is also shown (red dashed line).

Table 37: Exotica selection efficiency computed with the fit method as a function of photon η.

η	**MC**	**DATA**	R (DATA/MC)
0 - 0.5	90.63 ± 0.13 %	$86.85 \pm 0.63 \pm 1.78$ %	0.958 ± 0.039
0.5 - 1.0	91.02 ± 0.13 %	$88.62 \pm 0.60 \pm 1.99$ %	0.974 ± 0.008
1.0 - 1.4442	91.47 ± 0.14 %	$88.60 \pm 0.70 \pm 1.22$ %	0.969 ± 0.009
1.566 - 1.8	90.69 ± 0.21 %	$88.62 \pm 0.72 \pm 2.17$ %	0.978 ± 0.025
1.8 - 2.1	91.15 ± 0.20 %	$91.09 \pm 0.96 \pm 0.68$ %	0.999 ± 0.013
2.1 - 2.5	93.51 ± 0.17 %	$90.83 \pm 1.40 \pm 2.07$ %	0.971 ± 0.026

Table 38: Exotica selection efficiency in barrel and endcap computed with the fit method as a function of photon R9.

R9	**MC**	**DATA**	R (DATA/MC)
Barrel			
0 - 0.80	89.47 $\pm$ 0.15 %	85.56 $\pm$ 1.03 $\pm$ 2.00 %	0.956 $\pm$ 0.025
0.80 - 0.94	91.12 $\pm$ 0.13 %	88.38 $\pm$ 0.43 $\pm$ 0.61 %	0.970 $\pm$ 0.008
0.94 - 1.0	92.47 $\pm$ 0.14 %	89.91 $\pm$ 0.44 $\pm$ 0.43 %	0.973 $\pm$ 0.007
Endcap			
0 - 0.80	86.78 $\pm$ 0.33 %	82.52 $\pm$ 1.80 $\pm$ 1.52 %	0.951 $\pm$ 0.027
0.80 - 0.94	91.76 $\pm$ 0.17 %	91.50 $\pm$ 0.63 $\pm$ 1.06 %	0.997 $\pm$ 0.014
0.94 - 1.0	94.68 $\pm$ 0.16 %	93.75 $\pm$ 0.57 $\pm$ 0.45 %	0.990 $\pm$ 0.008

Table 39: Exotica selection efficiency in barrel and endap computed with the fit method as a function of photon $\mathrm{E/fbrem}$.

fBrem	**MC**	**DATA**	R (DATA/MC)
Barrel			
-0.2 - 0.2	90.34 $\pm$ 0.13 %	86.59 $\pm$ 0.79 $\pm$ 1.93 %	0.959 $\pm$ 0.023
0.2 - 0.6	91.34 $\pm$ 0.14 %	88.67 $\pm$ 0.63 $\pm$ 0.62 %	0.971 $\pm$ 0.009
0.6 - 1.0	91.42 $\pm$ 0.13 %	89.04 $\pm$ 0.56 $\pm$ 0.77 %	0.974 $\pm$ 0.010
Endcap			
-0.2 - 0.2	91.48 $\pm$ 0.30 %	85.20 $\pm$ 1.50 $\pm$ 2.12 %	0.931 $\pm$ 0.029
0.2 - 0.6	92.26 $\pm$ 0.17 %	91.69 $\pm$ 0.79 $\pm$ 0.98 %	0.994 $\pm$ 0.014
0.6 - 1.0	91.67 $\pm$ 0.18 %	90.80 $\pm$ 0.87 $\pm$ 1.80 %	0.990 $\pm$ 0.022

Table 40: Exotica selection efficiency in barrel and endcap computed with the opposite-same sign method as a function of photon $\mathrm{E_T}$.

$\mathrm{E_T}$	**MC**	**DATA**	R (DATA/MC)
Barrel			
20 - 35	86.97 $\pm$ 0.16 %	86.22 $\pm$ 0.48 $\pm$ 1.59 %	0.991 $\pm$ 0.019
35 - 45	92.21 $\pm$ 0.11 %	90.53 $\pm$ 0.34 $\pm$ 0.59 %	0.981 $\pm$ 0.008
45 - inf	93.61 $\pm$ 0.13 %	91.08 $\pm$ 0.44 $\pm$ 0.17 %	0.973 $\pm$ 0.005
Endcap			
20 - 35	88.54 $\pm$ 0.22 %	88.98 $\pm$ 0.60 $\pm$ 2.17 %	1.005 $\pm$ 0.025
35 - 45	93.20 $\pm$ 0.16 %	93.04 $\pm$ 0.48 $\pm$ 0.99 %	0.998 $\pm$ 0.012
45 - inf	94.94 $\pm$ 0.20 %	94.26 $\pm$ 0.66 $\pm$ 0.21 %	0.993 $\pm$ 0.007

Table 41: Exotica selection efficiency computed with the opposite-same sign method as a function of photon η.

η	**MC**	**DATA**	R (DATA/MC)
0 - 0.5	90.63 $\pm$ 0.13 %	88.57 $\pm$ 0.40 $\pm$ 1.24 %	0.978 $\pm$ 0.014
0.5 - 1.0	91.02 $\pm$ 0.13 %	89.73 $\pm$ 0.40 $\pm$ 0.59 %	0.986 $\pm$ 0.008
1.0 - 1.4442	91.47 $\pm$ 0.14 %	90.29 $\pm$ 0.44 $\pm$ 0.97 %	0.987 $\pm$ 0.012
1.566 - 1.8	90.69 $\pm$ 0.21 %	89.97 $\pm$ 0.67 $\pm$ 1.05 %	0.992 $\pm$ 0.014
1.8 - 2.1	91.15 $\pm$ 0.20 %	91.68 $\pm$ 0.58 $\pm$ 1.38 %	1.006 $\pm$ 0.016
2.1 - 2.5	93.51 $\pm$ 0.17 %	92.26 $\pm$ 0.54 $\pm$ 1.10 %	0.986 $\pm$ 0.013

Table 42: Exotica selection efficiency in barrel and endcap computed with the opposite-same sign method as a function of photon R9.

R9	**MC**	**DATA**	R (DATA/MC)
Barrel			
0 - 0.80	89.47 $\pm$ 0.15 %	88.52 $\pm$ 0.42 $\pm$ 1.95 %	0.989 $\pm$ 0.023
0.80 - 0.94	91.12 $\pm$ 0.13 %	89.48 $\pm$ 0.39 $\pm$ 0.36 %	0.982 $\pm$ 0.006
0.94 - 1.0	92.47 $\pm$ 0.14 %	90.05 $\pm$ 0.42 $\pm$ 0.14 %	0.974 $\pm$ 0.005
Endcap			
0 - 0.80	86.78 $\pm$ 0.33 %	87.08 $\pm$ 0.90 $\pm$ 3.65 %	1.003 $\pm$ 0.043
0.80 - 0.94	91.76 $\pm$ 0.17 %	90.96 $\pm$ 0.50 $\pm$ 0.30 %	0.991 $\pm$ 0.006
0.94 - 1.0	94.68 $\pm$ 0.16 %	93.75 $\pm$ 0.52 $\pm$ 0.11 %	0.990 $\pm$ 0.006

Table 43: Exotica selection efficiency in barrel and endcap computed with the opposite-same sign method as a function of photon $\mathrm{E}/\mathrm{fbrem}$.

fBrem	**MC**	**DATA**	R (DATA/MC)
Barrel			
-0.2 - 0.2	90.34 $\pm$ 0.13 %	88.72 $\pm$ 0.41 $\pm$ 2.10 %	0.982 $\pm$ 0.024
0.2 - 0.6	91.34 $\pm$ 0.14 %	89.65 $\pm$ 0.43 $\pm$ 0.37 %	0.981 $\pm$ 0.006
0.6 - 1.0	91.42 $\pm$ 0.13 %	90.03 $\pm$ 0.40 $\pm$ 0.31 %	0.985 $\pm$ 0.006
Endcap			
-0.2 - 0.2	91.48 $\pm$ 0.30 %	90.03 $\pm$ 0.99 $\pm$ 3.51 %	0.984 $\pm$ 0.040
0.2 - 0.6	92.26 $\pm$ 0.17 %	91.32 $\pm$ 0.53 $\pm$ 0.17 %	0.990 $\pm$ 0.006
0.6 - 1.0	91.67 $\pm$ 0.18 %	91.41 $\pm$ 0.51 $\pm$ 0.76 %	0.997 $\pm$ 0.010

Table 44: Exotica photon selection efficiency as a function of the number of reconstructed vertices in signal MC.

N vtx	**Efficiency**
Barrel	
1	91.93 $\pm$ 0.19 %
2	91.49 $\pm$ 0.13 %
3	90.98 $\pm$ 0.14 %
>=4	90.29 $\pm$ 0.13 %
Endcap	
1	93.23 $\pm$ 0.26 %
2	92.51 $\pm$ 0.19 %
3	92.45 $\pm$ 0.20 %
>=4	91.56 $\pm$ 0.19 %

C.5 High E_T behaviour of the Selection

Some analysis have applied the efficiency measurement done in the highest E_T bin to much more higher energies (up to TeV). We have therefore checked the behaviour of the selection at very high energies in order to determine possible additional sources of systematic error. Figure 26 shows the selection efficiency measured from MC for photons up to 1 TeV in barrel and endcap.

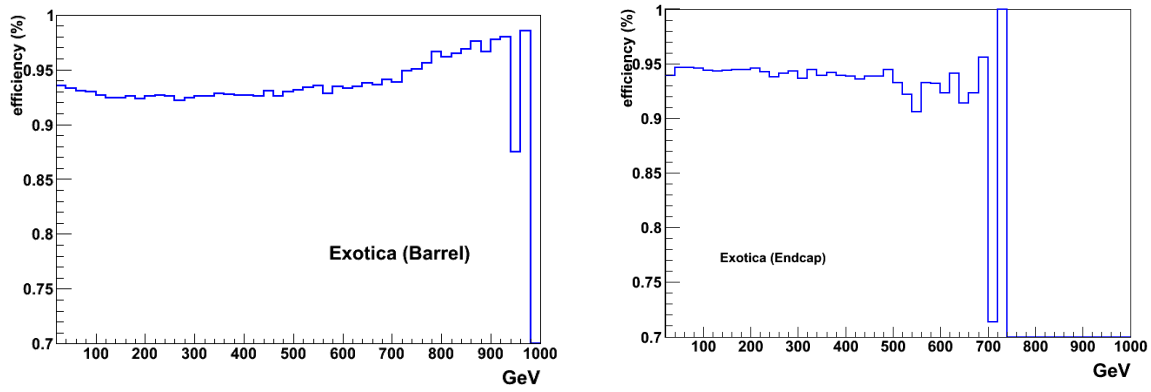

(a) (b)

Figure 26: Exotica selection efficiency estimated from MC for very high energy photons in barrel (a) and endcap (b).

In barrel the efficiency slowly decreases up to 500 GeV photon E_T. Then the energy dependant correction to the isolation threshold becomes of the order of few GeV loosening the corresponding cuts with the consequent increase in efficiency. In endcap the selection efficiency is quite flat as a function of the photon transverese energy. We suggest therefore to add to the systematic error 50% of the difference between the measured value and the extrapolation at high E_T.

D 3_9_X Results

The following tables report the efficiency measurements for Exotica, Conversion and Combined Isolation selections. Data used in the measurement was re-recoed with `CMSSW_3_9_X`. The MC samples used in the comparison have been simulated with `CMSSW_3_8_X`.

Table 45: Exotica Barrel

ET	MC	DATA	MC Ratio γ/e
20 - 35	87.41 $\pm$ 0.47 %	86.05 $\pm$ 0.45 $\pm$ 4.86 %	1.056 $\pm$ 0.003
35 - 45	92.27 $\pm$ 0.32 %	89.89 $\pm$ 0.35 $\pm$ 0.63 %	1.008 $\pm$ 0.004
45 - inf	93.63 $\pm$ 0.37 %	90.81 $\pm$ 0.42 $\pm$ 0.37 %	1.008 $\pm$ 0.005

D.1 Selection Efficiency in Various Run Ranges

The selection efficiencies have been measured in different run ranges corresponding to different set of trigger selection. Figure 27 show the results for Exotica, Conversion and Combined Isolation efficiencies. The effect of the varying pileup conditions is clear.

Table 46: Exotica Endcap

ET	MC	DATA	MC Ratio γ/e
20 - 35	88.93 $\pm$ 0.63 %	88.71 $\pm$ 0.58 $\pm$ 3.75 %	1.042 $\pm$ 0.003
35 - 45	93.40 $\pm$ 0.47 %	91.83 $\pm$ 0.51 $\pm$ 0.67 %	1.017 $\pm$ 0.005
45 - inf	95.07 $\pm$ 0.56 %	94.12 $\pm$ 0.58 $\pm$ 0.83 %	0.984 $\pm$ 0.005

Table 47: Conversion Barrel

ET	MC	DATA	MC Ratio γ/e
20 - 35	84.66 $\pm$ 0.51 %	82.36 $\pm$ 0.50 $\pm$ 3.35 %	1.052 $\pm$ 0.003
35 - 45	90.12 $\pm$ 0.35 %	86.70 $\pm$ 0.39 $\pm$ 0.48 %	1.023 $\pm$ 0.004
45 - inf	91.76 $\pm$ 0.42 %	87.50 $\pm$ 0.48 $\pm$ 0.25 %	1.008 $\pm$ 0.005

Table 48: Conversion Endcap

ET	MC	DATA	MC Ratio γ/e
20 - 35	88.88 $\pm$ 0.63 %	88.67 $\pm$ 0.58 $\pm$ 3.75 %	1.042 $\pm$ 0.003
35 - 45	93.34 $\pm$ 0.47 %	91.73 $\pm$ 0.52 $\pm$ 0.67 %	1.017 $\pm$ 0.005
45 - inf	95.03 $\pm$ 0.57 %	93.89 $\pm$ 0.58 $\pm$ 0.83 %	0.984 $\pm$ 0.005

Table 49: Combined Iso Barrel

ET	MC	DATA	MC Ratio γ/e
20 - 35	88.05 $\pm$ 0.46 %	85.45 $\pm$ 0.45 $\pm$ 3.40 %	1.049 $\pm$ 0.003
35 - 45	93.27 $\pm$ 0.30 %	90.18 $\pm$ 0.34 $\pm$ 0.50 %	1.022 $\pm$ 0.004
45 - inf	94.58 $\pm$ 0.35 %	90.31 $\pm$ 0.43 $\pm$ 0.25 %	1.002 $\pm$ 0.005

Table 50: Combined Iso Endcap

ET	MC	DATA	MC Ratio γ/e
20 - 35	87.95 $\pm$ 0.65 %	87.80 $\pm$ 0.61 $\pm$ 3.98 %	1.044 $\pm$ 0.003
35 - 45	94.40 $\pm$ 0.43 %	93.46 $\pm$ 0.47 $\pm$ 0.60 %	1.029 $\pm$ 0.005
45 - inf	96.62 $\pm$ 0.47 %	96.44 $\pm$ 0.45 $\pm$ 0.78 %	1.025 $\pm$ 0.005

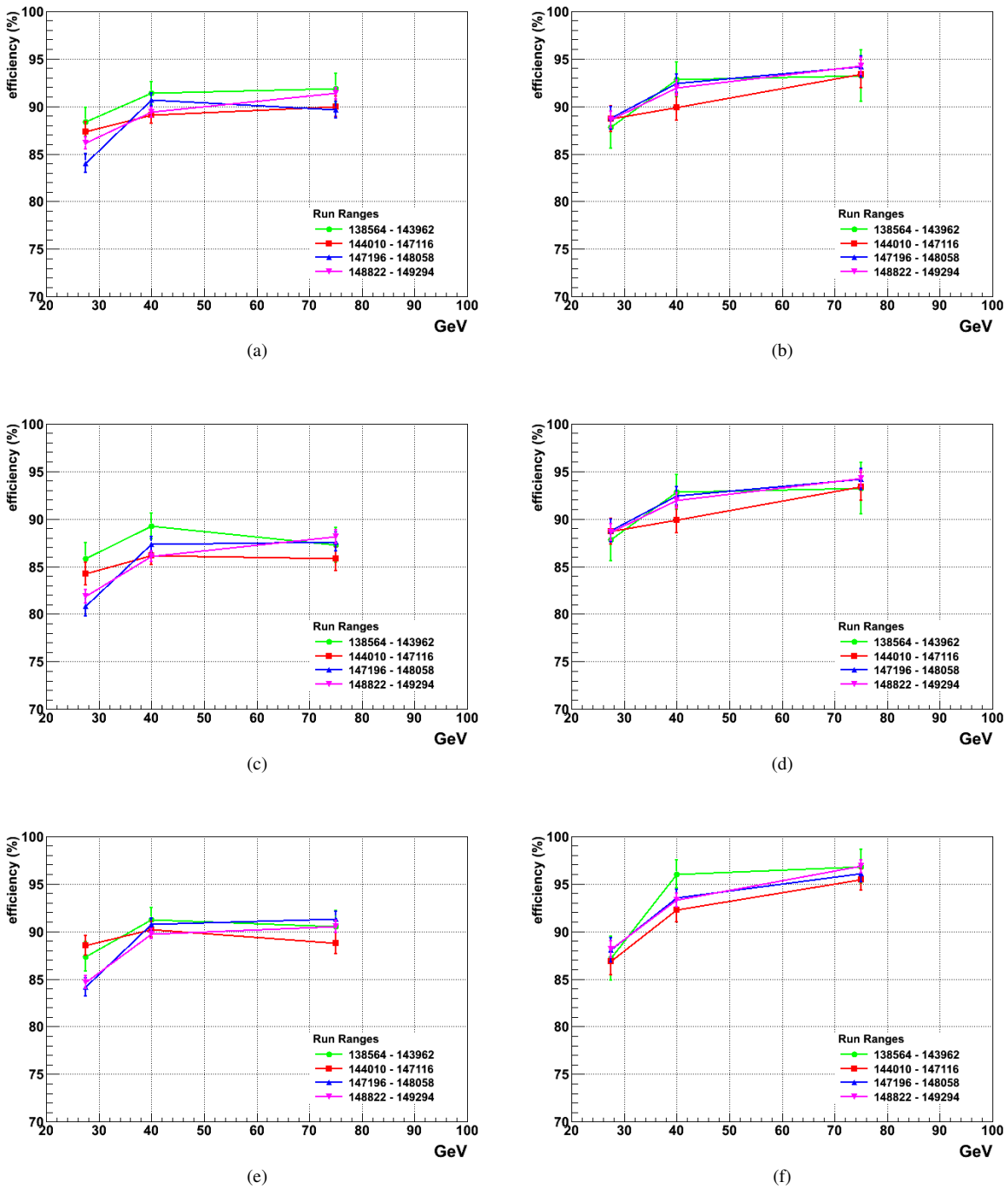

(a) (b) (c) (d) (e) (f)

Figure 27: Selection efficiency in barrel and endcap in different run ranges for Exotica (a) (b), Conversion (c) (d) and Combined Isolation (e) (f) selections.

References

[1] The CMS Collaboration, *Measuring Electron Efficiencies at CMS with Early Data*, CMS PAS EGM-07-001 (2007).

[2] *PYTHIA 6.4 Physics and Manual*, JHEP 05 (2006) 026.

[3] The CMS Collaboration, *Isolated Photon Reconstruction and Identification at* $sqrts = 7\,\mathrm{TeV/c^2}$, CMS PAS EGM-10-006 (2010).

[4] C. Jessop, T. Kolberg and N. Marinelli, *Isolated Photon Production Cross Section in pp collision ar sqrt(s) = 7 TeV using conversions.*, CMS AN-11-033 (2011).

[5] S. Ganjour et Al., *Measurement of Isolatied Photon Production Cross Section in pp collision ar sqrt(s) = 7 TeV with Isolation Template and 2010 Dataset.*, CMS AN-11-066 (2011).

[6] Bandurin D., Halyo V., Werner J. *Data Driven Techniques to Estimate the Background in the Z→ee Events*, CMS AN-2010/277

[7] Baffioni S. et Al., *Electron Identification in CMS*, CMS AN-2009/178, *https://twiki.cern.ch/twiki/bin/view/CMS/SWGuideCategoryBasedElectronID*.